Elsevier Editorial System(tm) for Journal of Hydrology

Manuscript Draft

Manuscript Number:

Title: Contributions of human activities to suspended sediment yield during storm events from a small, steep, tropical watershed

Article Type: Research Paper

Keywords: Sediment yield, volcanic islands, mountainous catchments, storm events, coastal sediment load, American Samoa

Corresponding Author: Mr. Alex Messina, M.S.

Corresponding Author's Institution: San Diego State University

First Author: Alex Messina, M.S.

Order of Authors: Alex Messina, M.S.; Trent W Biggs, Phd

Abstract: Suspended sediment yields (SSY) were measured during storm and non-storm periods from undisturbed and human-disturbed portions of a small (1.8 km²), mountainous watershed that drains to a sediment-stressed coral reef. Event-wise SSY (SSYEV) was calculated for 142 storms from measurements of water discharge (Q), turbidity (T), and suspended sediment concentration (SSC) measured downstream of three key sediment sources: undisturbed forest, an aggregate quarry, and a village. SSC and SSYEV were significantly higher downstream of the quarry during both storm- and non-storm periods. The human-disturbed subwatershed accounted for an average of 71-87% of SSYEV from the total watershed, and has increased loads to the coast by 1.7-3.9x over natural background. Specific SSY (tons/area) from the disturbed quarry area was 49x higher than from natural forest compared with 8x higher from the village. The quarry, which covers 1.1% of the total watershed area, contributed 36% of total SSYEV at the outlet. Similar to mountainous watersheds in semi-arid and temperate climates, SSYEV from both the undisturbed and disturbed watersheds correlated closely with maximum event discharge (Qmax), event total precipitation and event total Q, but not with a precipitation erosivity index. Best estimates of annual SSYEV varied from 41-61 tons/yr (45-68 tons/km²/yr) from the undisturbed subwatershed, 310-388 tons/yr (350-441 tons/km²/yr) from the human-disturbed subwatershed , and 360-439 tons/yr (200-247 tons/km2/yr) from the total watershed. Sediment yield was very sensitive to disturbance; only 5.2% of the watershed is disturbed by humans but sediment yield increased significantly (3.9x). While unpaved roads are often identified as a source of sediment in humid forested regions, field observations suggested that most roads in the urban area were stabilized with aggregate. Repeated surface disturbance at the quarry is a key process maintaining high rates of sediment generation. Given the large distance to other sources of building material, aggregate mining and associated sediment disturbance may be a critical sediment source on remote islands in the Pacific and elsewhere. Identification of sediment hotspots like the quarry using rapid, event-wise measures of suspended sediment yield will help efforts to mitigate sediment load and restore coral reefs.

Suggested Reviewers: Thomas Dunne
UC Santa Barbara Bren School
tdunne@bren.ucsb.edu

Clement Duvert
School of Earth, Environmental and Biological Sciences, Queensland University of Technology
clement.duvert@gmail.com

Murray Hicks
National Institute of Water and Atmospheric Research
Murray.Hicks@niwa.co.nz

Jonathan Warrick
US Geological Survey
jwarrick@usgs.gov

Carlos Ramos Scharron
University of Texas at Austin
cramos@austin.utexas.edu

Highlights (3 to 5 bullet points (maximum 85 characters including spaces per bullet point)

- Human disturbance increased SSY to Faga'alu Bay by 3.9x over pre-disturbance
- Qmax was a good predictor of storm SSY in disturbed and undisturbed watersheds
- rapidly developed an empirical SSY model for a remote, data-poor watershed

TITLE:

Contributions of human activities to suspended sediment yield during storm events from a small, steep, tropical watershed

Authors:

Messina, A.M.[a*], Biggs, T.W.[a]

[a] San Diego State University, Department of Geography, San Diego, CA 92182,

amessina@rohan.sdsu.edu, +1-619-594-5437, tbiggs@mail.sdsu.edu, +1-619-594-0902

ABSTRACT

Suspended sediment yields (SSY) were measured during storm and non-storm periods from undisturbed and human-disturbed portions of a small (1.8 km²), mountainous watershed that drains to a sediment-stressed coral reef. Event-wise SSY (SSY_{EV}) was calculated for 142 storms from measurements of water discharge (Q), turbidity (T), and suspended sediment concentration (SSC) measured downstream of three key sediment sources: undisturbed forest, an aggregate quarry, and a village. SSC and SSY_{EV} were significantly higher downstream of the quarry during both storm- and non-storm periods. The human-disturbed subwatershed accounted for an average of 71-87% of SSY_{EV} from the total watershed, and has increased loads to the coast by 1.7-3.9x over natural background. Specific SSY (tons/area) from the disturbed quarry area was 49x higher than from natural forest compared with 8x higher from the village. The quarry, which covers 1.1% of the total watershed area, contributed 36% of total SSY_{EV} at the outlet. Similar to mountainous watersheds in semi-arid and temperate climates, SSY_{EV} from both the undisturbed and disturbed watersheds correlated closely with maximum event discharge (Qmax), event total precipitation and event total Q, but not with a precipitation erosivity index. Best estimates of

annual SSY_{EV} varied from 41-61 tons/yr (45-68 tons/km²/yr) from the undisturbed subwatershed, 310-388 tons/yr (350-441 tons/km²/yr) from the human-disturbed subwatershed, and 360-439 tons/yr (200-247 tons/km^2/yr) from the total watershed. Sediment yield was very sensitive to disturbance; only 5.2% of the watershed is disturbed by humans but sediment yield increased significantly (3.9x). While unpaved roads are often identified as a source of sediment in humid forested regions, field observations suggested that most roads in the urban area were stabilized with aggregate. Repeated surface disturbance at the quarry is a key process maintaining high rates of sediment generation. Given the large distance to other sources of building material, aggregate mining and associated sediment disturbance may be a critical sediment source on remote islands in the Pacific and elsewhere. Identification of sediment hotspots like the quarry using rapid, event-wise measures of suspended sediment yield will help efforts to mitigate sediment load and restore coral reefs.

Keywords:

Sediment yield, volcanic islands, mountainous catchments, land use, storm events, coastal sediment load, American Samoa

Introduction

Human activities including deforestation, agriculture, road construction, mining, and urbanization alter the timing, composition, and amount of sediment loads to downstream ecosystems (Syvitski et al., 2005). Increased sediment loads can stress aquatic ecosystems, including coral reefs that occur near the outlets of impacted watersheds. Sediment impacts coral by decreasing light for photosynthesis and increasing sediment accumulation rates (Fabricius, 2005; Storlazzi et al., 2015; West and van Woesik, 2001). Anthropogenic sediment disturbance

45 can be particularly high on volcanic islands in the humid tropics, which have a high potential for
46 erosion due to high rainfall, extreme weather events, steep slopes, and erodible soils. Sediment
47 yield in densely vegetated watersheds can be particularly sensitive to land clearing, which alters
48 the fraction of exposed soil more than in sparsely-vegetated regions. The steep topography and
49 small floodplains on small volcanic islands further limits sediment storage and the capacity of
50 the watershed to buffer increased hillslope sediment supply. Such environments characterize
51 many volcanic islands in the south Pacific where coral reefs are impacted by sediment.

52 A large proportion of a watershed's sediment yield can originate from disturbed areas that
53 cover a relatively small fraction of the watershed area. In the Caribbean, unpaved roads covering
54 0.3-0.9% of the watershed area were the dominant sediment source in disturbed watersheds on
55 St. John, and increased sediment yield to the coast by 5-9 times relative to undisturbed
56 watersheds (Ramos-Scharrón and Macdonald, 2007). In the Pacific Northwest of the United
57 States, several studies found most road-generated sediment can originate from just a small
58 fraction of unpaved roads (Gomi et al., 2005; Henderson and Toews, 2001; Megahan et al., 2001;
59 Wemple et al., 1996), and heavily used roads could generate 130 times as much sediment as
60 abandoned roads (Reid and Dunne, 1984). In a watershed disturbed by grazing on Molokai,
61 Hawaii, less than 5% of the land produces most of the sediment, and only 1% produces
62 approximately 50% of the sediment (Risk, 2014; Stock et al., 2010), suggesting that management
63 should focus on identifying, quantifying, and mediating erosion hotspots.

64 Management of sediment requires linking land use changes and mitigation strategies to
65 changes in sediment yields at the watershed outlet (Walling and Collins, 2008). A sediment
66 budget quantifies sediment as it moves from key sources like hillslope erosion, channel-bank
67 erosion, and mass movements, to its eventual exit from a watershed (Rapp, 1960). Walling

(1999) used a sediment budget to show that sediment yield from watersheds can be insensitive to both land use change and erosion management due to high sediment storage capacity on hillslopes and in the channel. Sediment yield from disturbed areas can be large but may not be important compared to naturally high yields from undisturbed areas. While a full description of all sediment production and transport processes are of scientific interest, the sediment budget needs to be simplified to be used as a management tool (Slaymaker, 2003). Most management applications require only that the order of magnitude or the relative importance of process rates be known, so Reid and Dunne (1996) argue a management-focused sediment budget can be developed quickly in situations where the management problem is clearly defined and the management area can be divided into homogenous sub-units.

Knowledge of suspended sediment yield (SSY) under both natural and disturbed conditions on most tropical, volcanic islands remains limited, due to the challenges of in situ monitoring in these remote, challenging environments. The limited data has also made it difficult to develop reliable sediment yield models for ungauged watersheds. Existing sediment yield models are often designed for agricultural landscapes and are not well-calibrated to the climatic, topographic, and geologic conditions found on steep, tropical islands. Most readily available models also do not incorporate many of the important processes that generate sediment in steep watersheds, including mass movements (Calhoun and Fletcher, 1999; Ramos-Scharrón and Macdonald, 2005; Sadeghi et al., 2007). Developing models that predict SSY_{EV} from small, mountainous catchments is a significant contribution for establishing baselines for change-detection for sediment mitigation projects, and can also further improve models applied at the regional scale (Duvert et al., 2012).

Traditional approaches to quantifying human impact on sediment budgets, including comparison of total annual yields (Fahey et al., 2003) and sediment rating curves (Asselman, 2000; Walling, 1977), are complicated by interannual climatic variability and hysteresis in the discharge-concentration relationship. Sediment yield can be highly variable over various time scales, even under natural conditions. At geologic time scales, if an undisturbed watershed is not in a steady-state condition, sediment yields may decrease over time as it reaches equilibrium, or the sediment contributions from different subwatersheds may change with time (Ferrier et al., 2013; Perroy et al., 2012). At decadal scales, cyclical climatic variability like El Nino-Southern Oscillation (ENSO) events or Pacific Decadal Oscillation (PDO) patterns can significantly alter sediment yield from undisturbed watersheds (Wulf et al., 2012).

As an alternative to comparing annual sediment loads, SSY generated by storm events of the same magnitude can be compared to assess the contribution of individual subwatersheds to total SSY (Zimmermann et al., 2012), determine changes in SSY from the same watershed over time (Bonta, 2000), and compare the responses of different watersheds to various precipitation or discharge variables ("storm metrics") (Basher et al., 2011; Duvert et al., 2012; Fahey et al., 2003; Hicks, 1990). Event-wise SSY (SSY_{EV}) may correlate with storm metrics such as total precipitation, the Erosivity Index (Kinnell, 2013), or total discharge, but the best correlation has consistently been found with maximum event discharge (Qmax). Several researchers have hypothesized that Qmax integrates the hydrological response of a watershed, making it a good predictor of SSY_{EV} in diverse environments (Duvert et al., 2012; Rankl, 2004). High correlation between SSY_{EV} and Qmax has been found in semi-arid, temperate, and sub-humid watersheds in Wyoming (Rankl, 2004), Mexico, Italy, France (Duvert et al., 2012), and New Zealand (Basher

et al., 2011; Hicks, 1990), but this approach has not been attempted for steep, tropical watersheds on volcanic islands.

The anthropogenic impact on SSY_{EV} may vary by storm magnitude, as documented in Pacific Northwest forests (Lewis et al., 2001). As storm magnitude increases, water yield and/or SSY_{EV} from natural areas may increase relative to human-disturbed areas, diminishing anthropogenic impact relative to the natural baseline. While large storms account for most SSY under undisturbed conditions, human-disturbed areas may show the largest disturbance, expressed as a percentage increase above the natural background, for smaller storms (Lewis et al., 2001). The disturbance ratio (DR) may be highest for small storms, when background SSY_{EV} from the undisturbed forest is low and erodible sediment from disturbed surfaces is the dominant source. For large storms, mass movements and bank erosion may contribute to naturally high SSY_{EV} from undisturbed watersheds, increasing the background and reducing the DR for large events.

This study uses in situ measurements of precipitation (P), stream discharge (Q), turbidity (T) and suspended sediment concentration (SSC) to 1) quantify suspended sediment yield from undisturbed and human-disturbed portions of a small watershed in the south Pacific and 2) develop an empirical model of storm-generated suspended sediment yield. The questions addressed include: How much has human disturbance increased suspended sediment yield to the coast? What human activities dominate the anthropogenic contribution to the suspended sediment load? Which storm metric is the best predictor of storm event suspended sediment yield (SSY_{EV}): total event precipitation, Erosivity Index, total event discharge, or maximum event discharge? How do sediment contributions from undisturbed areas and human-disturbed areas vary with storm size?

Study Area

The study watershed, Faga'alu, is located on Tutuila (14S, 170W), the largest island in the Territory of American Samoa (140 km²). Like many volcanic islands in the Pacific, Tutuila has steep, heavily forested mountains with villages and roads mostly confined to the flat areas near the coast. The main stream in Faga'alu runs the length of the watershed (~3 km), and drains an area of 1.78 km² into Faga'alu Bay (area draining to FG3 in Figure 1). The main watershed includes Matafao Mountain, the highest point on Tutuila (653 m). The mean slope of the main Faga'alu watershed is 0.53 m/m and total relief is 653 m. The administrative boundary includes the watersheds of the main stream and several small ephemeral streams that drain directly to the bay (0.63 km²) (grey dotted boundary in Figure 1). The coral reef in Faga'alu Bay is highly degraded by sediment (Fenner et al., 2008). Faga'alu watershed was identified by local environmental management agencies in the American Samoa Coral Reef Advisory Group (CRAG) as a heavily impacted watershed, and in August 2012 was selected by the US Coral Reef Task Force (USCRTF) as a Priority Watershed for conservation and remediation efforts (Holst-Rice et al., 2015).

Faga'alu occurs on intracaldera Pago Volcanics where the K-Ar age for a sample in the watershed is 1.20 Mya (McDougall, 1985). Soil types in the steep uplands are Fagasa family-lithic hapludolls with rock outcrops in the steep uplands, and soil types in the lowlands are Aua-Leafu complex (Nakamura, 1984). In the uplands, an estimated 50% of soil cover is Fagasa family soils which are moderately deep and well drained silty clay (50-150 cm) overlying weathered igneous bedrock. An estimated 20% of soil cover is lithic hapludolls which are well drained but shallower (10-50 cm) than Fagasa family soil, and composed of silty clay and clay loam. The remaining 15% of soil in the uplands is rock outcrops. The lowlands are composed of

158 urban surfaces and a mix of Aua and Leafu soils, composed of colluvium and alluvium derived
159 from the weathered igneous rock and soil from the steep uplands. Aua soils in the lowlands are
160 deep (>150 cm), well drained accumulations of very stony silty clay loam with only moderate
161 runoff and erosion potential. Leafu soils in the lowlands are very deep (>150 cm), poorly drained
162 silty clay to fine sandy loam that are typically along streams and valley bottoms where the high
163 water table is typically 90-150 cm deep.

164 ## Climate

165 Precipitation on Tutuila is caused by several mechanisms including cyclones and tropical
166 depressions, isolated thunderstorms, and orographic uplifting of trade-wind squalls over the high
167 (300-600 m), mountainous ridge that runs the length of the island. The ridge runs parallel to the
168 predominant wind direction, and does not cause a significant windward/leeward rainfall gradient
169 like many other Pacific Islands (Ferrier et al., 2013; Menking et al., 2013). Average annual
170 specific discharge ($m^3/yr/km^2$) shows little spatial variation across the island, irrespective of
171 watershed location or orientation (Dames & Moore, 1981). Precipitation increases with
172 elevation, from an average 2,380 mm/yr at the shoreline to 6,350 mm/yr at the highest elevation
173 on the island, averaging 3,800 mm/yr over the island from 1903 to 1973 (Eyre, 1989; Izuka et al.,
174 2005). In Faga'alu watershed, rainfall records show average annual precipitation is 6,350 mm at
175 Matafao Mtn. (653 m m.a.s.l), 5,280 mm at Matafao Reservoir (249 m m.a.s.l.) and about 3,800
176 mm on the coastal plain (Craig, 2009; Dames & Moore, 1981; Perreault, 2010; Tonkin & Taylor
177 International Ltd., 1989; Wong, 1996). Mean annual potential evapotranspiration follows the
178 opposite trend, varying from 890 mm at high elevation to 1,150 mm at sea level (Izuka et al.,
179 2005). Tropical cyclones are erratic but occurred on average every 1-13 years from 1981-2014

(Craig, 2009) and bring intense rainfall, flooding, landslides, and high sediment yield (Buchanan-Banks, 1979).

There are two subtle rainfall seasons: a drier winter season, from June through September and a wetter summer season, from October through May (Izuka et al., 2005). During the drier winter season, the island is influenced by relatively stronger, predominantly east to southeast trade winds, lower temperatures, lower humidity and lower total rainfall. During the wetter summer season the Inter-Tropical Convergence Zone (ITCZ) moves over the region, causing light to moderate Northerly winds, higher temperatures, higher humidity, and higher total rainfall. While total rainfall is lower in the drier tradewind season, large storm events are still observed. Analysis of 212 peak discharges at 11 continuous-record gaging sites 1959-1990 showed 65% of annual peak flows occurred during the wet season and 35% of annual peak flows occurred during the drier Tradewind season (Wong, 1996). Analysis of mean monthly rainfall data for the period 1971-2000 showed that 75% of precipitation occurred in the wet season, which includes 67% of the year (October-May), and 25% occurred in the dry season, which covers 33% of the year (June-September) (Perreault, 2010; data from USGS rain gauges and Parameter-elevation Relationships on Independent Slopes Model (PRISM) Climate Group (Daly et al., 2008)).

Land Cover and Land Use

The predominant land cover in Faga'alu watershed is undisturbed vegetation (94.8%), including forest (85.7%) and scrub/shrub (9.0%) on the steep hillsides (Table 1), based on a 1 m^2-resolution land cover map from NOAA's Ocean Service and Coastal Services Center (2010). The upper watershed, draining to FG1 in Figure 1, is dominated by undisturbed rainforest on steep hillslopes. The lower subwatershed, draining areas between FG1 and FG3 in Figure 1, has

steep vegetated hillslopes and a relatively small flat area in the valley bottom that is urbanized. This settlement pattern is typical in the South Pacific and other volcanic islands, where their small size and steep topography constrain development to valley bottoms near the coast (Bégin et al., 2014). Compared to other watersheds on Tutuila, a relatively large portion of Faga'alu watershed is urbanized (3.2% "High Intensity Developed" in Table 1), due to large areas of impervious surface associated with the hospital and the numerous residences and businesses. A small portion of the watershed (0.9%) is developed open space, which includes landscaped lawns and parks. In addition to some small household gardens there are several small agricultural areas of banana and taro on the steep hillsides. These agricultural plots were classified as grassland (0.2% GA, Table 1) due to the high fractional grass cover in the plots. Farmers of these plots receive technical assistance from the Natural Resource Conservation Service (NRCS) to mitigate erosion. There are several small footpaths and unpaved driveways in the village, but most unpaved roads are stabilized with compacted gravel and do not appear to be a major contributor of sediment (Horsley-Witten, 2012). Longitudinal sampling of Faga'alu stream during low flow conditions in 2011 showed significantly increased turbidity downstream of a bridge construction site on the village road approximately 200 m downstream of FG2 (Curtis et al., 2011). Construction of the bridge was completed in March 2012 and no longer increases turbidity.

An open-pit aggregate quarry covers 1.6 ha and accounts for the majority of the bare land, which covers 1.1% of the Faga'alu watershed (Table 1). The quarry has been in continuous operation since the 1960's by advancing into the steep hillside to quarry the underlying basalt formation (Latinis et al., 1996). The overburden of soil and weathered rock was either piled up on-site where it was eroded by storms, or was manually rinsed from crushed aggregate. With few sediment runoff controls in place, sediment was discharged directly to Faga'alu stream. In 2011,

226 the quarry operators installed some sediment runoff management practices such as silt fences and
227 settling ponds (Horsley-Witten, 2011) but they were unmaintained and inadequate to control the
228 large amount of sediment mobilized during storm events (Horsley-Witten, 2012). During the
229 study period (2012-2014), additional sediment control measures were installed and some large
230 piles of overburden were naturally overgrown by vegetation (Figure 2), altering the sediment
231 availability. In late 2014, large sediment retention ponds were installed to mitigate sediment
232 runoff and work is underway to document the reduction in sediment loading (Messina and Biggs,
233 forthcoming; See Holst-Rice et al. (2015) for a full description of sediment mitigation efforts at
234 the quarry).

235 Three water impoundment structures were built in the early 20th century in the upper part
236 of the watershed for drinking water supply and hydropower but only the highest, Matafao
237 Reservoir, was ever connected to the municipal water system and has since fallen out of use
238 (Tonkin & Taylor International Ltd., 1989) (Figure 1). The dam at point FG1 has filled with
239 bedload sediment and flows over the spillway even at the lowest flows. We assume the other
240 reservoirs are similarly filled with coarse sediment and are not currently retaining fine suspended
241 sediment. A full description of stream impoundments is in Appendix 1.

242 ## Methods

243 The suspended sediment yield (SSY) in Faga'alu stream was measured at three sampling
244 points that drain key land covers we hypothesized would have different SSY: FG1 drains
245 undisturbed forest in the UPPER subwatershed (watershed boundary to FG1), FG2 drains
246 undisturbed forest and the quarry in the LOWER_QUARRY subwatershed (between FG1 and
247 FG2), and FG3 drains undisturbed forest and the village in the LOWER_VILLAGE

248 subwatershed (between FG2 and FG3) (Table 1). FG3 is also the watershed outlet for the
249 TOTAL watershed.

250 ### Calculating suspended sediment yield from individual storm events (SSY_{EV})

251 SSY_{EV} at FG1, FG2, and FG3 were calculated by integrating continuous estimates of
252 SSY, calculated from measured or modeled water discharge (Q) and measured or modeled
253 suspended sediment concentration (SSC) (Duvert et al., 2012):

$$SSY_{EV} = k \int_{t=0}^{T} Q(t) * SSC(t) * dt \qquad \text{Equation 1}$$

where SSY_{EV} is suspended sediment yield (tons) for an event from t=0 at storm start to T=storm end, SSC is suspended sediment concentration (mg/L), and Q is water discharge (L/sec), and k converts from mg to tons (10^{-6}).

254 Storm events can be defined by precipitation (Hicks, 1990) or discharge parameters
255 (Duvert et al., 2012), and the method used to identify storm events on the hydrograph can
256 significantly influence the analysis of SSY_{EV} (Gellis, 2013). Dunne and Leopold (1978) assert
257 that all hydrograph separation schemes are arbitrary and usually have little to do with the
258 processes that generate storm flow, but if a consistent method is used then at least the results of
259 different analyses can be compared. Graphical techniques may be implemented to separate the
260 hydrograph into baseflow and quickflow, using the start and end of quickflow as the start and
261 end of the storm event (Dunne and Leopold, 1978; Perreault, 2010). Storms can also be filtered
262 from the analysis by using various criteria such as minimum storm duration, time between
263 discharge peaks, minimum peak discharge, or more complex schemes using statistical
264 distributions of flow percentiles (Gellis, 2013; Lewis et al., 2001). More complex signal
265 processing methods can also be used, including finding the inflection point of the second

266 derivative of the hydrograph to determine the end of the storm event. However, complex events
267 occur where subsequent precipitation generates stormflow before the stream has returned to
268 baseflow. In these cases, the storm definition scheme can significantly affect the analysis of
269 storm sediment yields by separating or combining multiple hydrograph peaks. Due to the high
270 number of storm events and the prevalence of complex storm events recorded at the study site,
271 an automated approach that robustly separated complex events was desirable. The storm
272 definition approach used in this study performed baseflow separation with a digital filter signal
273 processing technique (Nathan and McMahon, 1990) embedded in the R-statistical package
274 EcoHydRology (Fuka et al., 2014). Only events with quickflow for at least one hour and peak
275 flow greater than 10% of baseflow were included in the analysis. This approach was easily
276 automated for application to a large number of events, and adequately separated complex storm
277 events with multiple hydrograph peaks (See Appendix 3 for example).

278 ## Data Collection Methods

279 Data on precipitation (P), water discharge (Q), suspended sediment concentration (SSC)
280 and turbidity (T) were collected during four field campaigns: January-March, 2012, February-
281 July 2013, January-March 2014, and October-December 2014, and several intervening periods of
282 unattended monitoring by instruments with data loggers. Field sampling campaigns were
283 scheduled to coincide with the period of most frequent storms in the November-May wet season,
284 though large storms were sampled throughout the year.

285 ### *Precipitation*

286 Precipitation (P) was measured at three locations in Faga'alu watershed using Rainwise
287 RAINEW tipping-bucket rain gages (RG1 and RG2) and a Vantage Pro Weather Station (Wx)
288 (Figure 1). Data at RG2 was only recorded January-March, 2012, to determine a relationship

between elevation and precipitation in the LOWER subwatershed. While previous data suggest that precipitation increases with elevation (Izuka et al., 2005), here we do not calculate watershed-mean precipitation, and instead use precipitation depth at RG1 to indicate the depth of rainfall during a storm event. Most sheetwash and rill erosion, which depends on rainfall intensity and erosivity, occurred at the quarry, near the location of RG1. Rainfall data from RG1 is therefore most representative of rainfall at the quarry. The total event precipitation (Psum) and event Erosivity Index (EI30) were calculated using data from RG1, with data gaps filled by 15 min interval precipitation data from Wx.

Water Discharge

Stream gaging sites were chosen to take advantage of an existing control structure (FG1) and a stabilized stream cross section (FG3) (Duvert et al, 2010). At FG1 and FG3, Q was calculated from stream stage measurements taken at 15 minute intervals and a stage-Q rating curve calibrated to manual Q measurements. Q was measured in the field under both baseflow and stormflow conditions by the area-velocity method (AV) using a Marsh-McBirney flowmeter to measure flow velocity and channel surveys of cross-sectional area (Harrelson et al., 1994; Turnipseed and Sauer, 2010). The highest recorded stage was higher than the highest stage with measured Q, so the stage-Q rating at FG3 was extrapolated using Manning's equation, calibrating Manning's n (0.067) to the Q measurements. At FG1, the flow control structure is a masonry ogee spillway crest of a defunct stream capture. Since the highest recorded stage (120 cm) was higher than the highest stage with measured Q (17 cm), and the flow structure did not meet the assumptions for using Manning's equation to predict flow, the HEC-RAS model was used to create the stage-Q relationship (Brunner, 2010). See Appendix 2 for details of the cross sections and rating curves.

A suitable site for stream gaging was not present at the outlet of the LOWER_QUARRY subwatershed (FG2), so water discharge at FG2 was calculated as the product of the specific water discharge from FG1 (m^3/0.9 km^2) and the watershed area draining to FG2 (1.17 km^2). This assumes that specific water discharge from the subwatershed above FG2 is similar to above FG1. Discharge may be higher from the quarry surface, which represents 5.7% of the LOWER_QUARRY subwatershed, so Q, and thus SSY from the quarry are a conservative, lower bound estimate, particularly during small events when specific discharge from the UPPER watershed was small relative to specific discharge from the quarry. The quarry surface is continually being disturbed, sometimes with large pits excavated and refilled in the course of weeks, as well as intentional water control structures implemented over time. Given the changes in the contributing area of the quarry, estimates of water yield from the quarry were uncertain, so we assumed a uniform specific discharge for the whole LOWER_QUARRY subwatershed.

Continuous Suspended Sediment Concentration

Continuous SSC at 15 minute intervals was estimated from 1) linear interpolation of SSC measured from water samples, and 2) 15 min interval turbidity data (T) and a T-SSC relationship calibrated to stream water samples collected over a range of Q and SSC.

Stream water samples were collected by grab sampling with 500 mL HDPE bottles at FG1, FG2, and FG3. At FG2, water samples were also collected at 30 min intervals during storm events by an ISCO 3700 Autosampler triggered by a stage height sensor. Samples were analyzed for SSC on-island using gravimetric methods (Gray, 2014; Gray et al., 2000). Water samples were vacuum filtered on pre-weighed 47mm diameter, 0.7 um Millipore AP40 glass fiber filters, oven dried at 100 C for one hour, cooled and weighed to determine SSC (mg/L).

Interpolation of SSC values from grab samples could only be performed if at least three stream water samples were collected during a storm event (Nearing et al., 2007), and if an SSC sample was collected within 30 minutes of peak Q. SSC was assumed to be zero at the beginning and end of each storm if no grab sample data was available for those times (Lewis et al., 2001).

Turbidity (T) was measured at FG1 and FG3 using three types of turbidimeters: 1) Greenspan TS3000 (TS), 2) YSI 600OMS with 6136 turbidity probe (YSI), and 3) Campbell Scientific OBS500 (OBS). All turbidimeters were permanently installed in protective PVC housings near the streambed where the turbidity probe would be submerged at all flow conditions, with the turbidity probe oriented downstream. Despite regular maintenance, debris fouling during storm and baseflows was common and caused data loss during several storm events (Lewis et al., 2001).

The T-SSC relationship can be unique to each region, stream, instrument or even each storm event (Lewis et al., 2001), and can be influenced by water color, dissolved solids and organic matter, temperature, and the shape, size, and composition of sediment. However, T has proved to be a robust surrogate measure of SSC in streams (Gippel, 1995), and is most accurate when a unique T-SSC relationship is developed for each instrument separately, using in situ grab samples under storm conditions (Lewis, 1996). A unique T-SSC relationship was developed for each turbidimeter, at each location, using T data and SSC samples from storm periods only (r^2 values 0.79-0.99). See Appendix 4 for details on the T-SSC relationships.

Cumulative Probable Error (PE)

Uncertainty in SSY_{EV} estimates arises from both measurement and model errors, including stage-Q and T-SSC (Harmel et al., 2006). The Root Mean Square Error (RMSE) method estimates the "most probable value" of the cumulative or combined error by propagating

the error from each measurement and modeling procedure to the final SSY_{EV} calculation (Topping, 1972). The resulting cumulative probable error (PE) is the square root of the sum of the squares of the maximum values of the separate errors:

$$PE = \sqrt{\sum (E_{Qmeas}^2 + E_{SSCmeas}^2) + (E_{Qmod}^2 + E_{SSCmod}^2)} \quad \text{Equation 2}$$

where *PE* is the cumulative probable error for individual measured values (±%), E_{Qmeas} is uncertainty in Q measurements (±%), $E_{SSCmeas}$ is uncertainty in SSC measurements (± %), E_{Qmod} is uncertainty in Q modeled by the Stage-Q relationship (RMSE, as ±% of the mean observed Q), E_{SSCmod} is uncertainty in SSC modeled by the T-SSC relationship (RMSE, as ± % of the mean observed SSC) (Harmel et al., 2009).

E_{Qmeas} and $E_{SSCmeas}$ were estimated using lookup tables from the DUET-H/WQ software tool (Harmel et al., 2009). The effect of uncertain SSY_{EV} estimates may complicate conclusions about contributions from subwatersheds, anthropogenic impacts, and SSY_{EV}-Storm Metric relationships. This is common in sediment yield studies where successful models estimate SSY with ±50-100% accuracy (Duvert et al., 2012) but the difference in SSY from undisturbed and disturbed areas was expected to be much larger than the cumulative uncertainty. PE was calculated for SSY_{EV} from the UPPER and TOTAL watersheds, but not calculated for SSY_{EV} from the LOWER subwatershed since it was calculated as the difference of SSY_{EV_UPPER} and SSY_{EV_TOTAL}.

Relationship of sediment load to sediment budget

We use the measured sediment yield at three locations to quantify the in-stream suspended sediment budget. Other components of sediment budgets include channel erosion and or channel and floodplain deposition (Walling and Collins, 2008). Sediment storage and

remobilization can significantly complicate the interpretation of in-stream loads, and complicate the identification of a land use signal. In Faga'alu, the channel bed is predominantly large volcanic cobbles and coarse gravel, with no significant deposits of fine sediment. Upstream of the village, the valley is very narrow with no floodplain. In the downstream reaches of the lower watershed, where fines might deposit in the floodplain, the channel has been stabilized with cobble reinforced by fencing, so overbank flows and sediment deposition on the floodplain are not observed. We therefore assume that channel erosion and channel and floodplain deposition are insignificant components of the sediment budget, so the measured sediment yields at the three locations reflect differences in hillslope sediment supply. Minimal sediment storage also reduces the lag time between landscape disturbance and observation of sediment at the watershed outlet.

Quantifying SSY from disturbed and undisturbed subwatersheds

A main objective for this study was to quantify anthropogenic changes in SSY_{EV_TOTAL} as measured at FG3. Relative contributions to SSY_{EV_TOTAL} from undisturbed and human-disturbed areas were assessed using two approaches: 1) comparing SSY_{EV} contributions from subwatersheds for each storm and the average of all storms, and 2) the Disturbance Ratio (DR).

The percent contributions of subwatersheds to SSY_{EV_TOTAL} were calculated from SSY_{EV} measured at FG1, FG2, and FG3 (Figure 1). SSY_{EV} from the UPPER subwatershed was measured at FG1 ($SSY_{EV\_UPPER} = SSY_{EV\_FG1}$). SSY_{EV} from the LOWER subwatershed was calculated as $SSY_{EV\_LOWER}=SSY_{EV\_FG3}-SSY_{EV\_FG1}$. Where SSY_{EV} data at FG2 were also available, the contributions from the quarry subwatershed ($SSY_{EV\_LOWER\_QUARRY} = SSY_{EV\_FG2}-SSY_{EV\_FG1}$), and village subwatershed ($SSY_{EV\_LOWER\_VILLAGE} = SSY_{EV\_FG3}-SSY_{EV\_FG2}$) were calculated separately.

396 Land cover in the LOWER subwatershed includes both undisturbed and human-disturbed
397 surfaces. To calculate SSY_{EV} from disturbed areas, SSY_{EV} from undisturbed areas was estimated
398 using the specific SSY_{EV} ($sSSY_{EV}$ tons/km²) from the UPPER subwatershed multiplied by the
399 undisturbed area in the LOWER subwatershed:

$$SSY_{EV\_distrb} = SSY_{EV\_subws} - \left(sSSY_{EV\_UPPER} * Area_{undist}\right) \quad \text{Equation 3}$$

where SSY_{EV_distrb} is SSY_{EV} from disturbed areas only (tons), SSY_{EV_subws} is SSY_{EV} (tons) measured from the disturbed subwatershed (e.g. SSY_{EV_FG3}- SSY_{EV_FG2}), $sSSY_{EV\_UPPER}$ is specific SSY_{EV} (tons/km2) from the UPPER subwatershed (SSY_{EV_FG1}), and $Area_{undist}$ is the area of undisturbed forest in the disturbed subwatershed (km^2).

400 The disturbance ratio (DR) is the ratio of SSY_{EV} from the watershed under current
401 conditions to SSY_{EV} under pre-disturbance conditions, estimated using $sSSY_{UPPER}$:

$$DR = \frac{SSY_{EV\_subw}}{A_{subw} * sSSY_{EV\_UPPER}} \quad \text{Equation 4}$$

where A_{subw} is the cumulative watershed area of the subwatershed.

402 Both Equation 3 and 4 assume that the whole watershed was originally covered in forest,
403 and $sSSY_{EV}$ from forested areas in the LOWER subwatershed equals $sSSY_{EV}$ from the
404 undisturbed UPPER watershed. SSY_{EV} from the disturbed portions of the LOWER subwatershed
405 (Equation 3) was used to calculate a DR for just the disturbed areas in the LOWER
406 subwatershed.

407 ### Predicting event suspended sediment yield (SSY_{EV})

408 Four storm metrics were tested as predictors of SSY_{EV}: total event precipitation (Psum),
409 event Erosivity Index (EI30) (Hicks, 1990; Kinnell, 2013), total event water discharge (Qsum),
410 and maximum event water discharge (Qmax) (Duvert et al., 2012; Rodrigues et al., 2013).

411 SSY_{EV} and the discharge metrics (Qsum and Qmax) were normalized by watershed area to
412 compare different sized watersheds.

413 The relationship between SSY_{EV} and storm metrics is often best fit by a power law
414 function:

$$SSY_{EV} = \alpha X^{\beta} \quad \text{Equation 5}$$

where X is a storm metric, and the regression coefficients α and β are obtained by ordinary least squares regression on the logarithms of SSY_{EV} and X (Basher et al., 2011; Duvert et al., 2012; Hicks, 1990). Model fits for each storm metric were compared using coefficients of determination (r^2) and Root Mean Square Error (RMSE). The correlation between storm metrics (X) and SSY_{EV} was also quantified using both parametric (Pearson) and non-parametric (Spearman) correlation coefficients.

415 The regression coefficients (α and β) for the UPPER and TOTAL watersheds were tested
416 for statistically significant differences using Analysis of Covariance (ANCOVA) (Lewis et al.,
417 2001). A higher intercept (α) for the human-disturbed watershed indicates higher sediment yield
418 for the same size storm event, compared to sediment yield from undisturbed areas. A difference
419 in slope (β) would indicate the relative sediment contributions from the subwatersheds change
420 with increasing storm size. If regression slopes for the UPPER and TOTAL watersheds are
421 significantly different, it supports the conclusion that the effect of human-disturbance changes
422 with storm size.

423 ### Annual estimates of SSY and sSSY

424 Annual estimates of SSY and sSSY were calculated to compare Faga'alu with other
425 watersheds reported in the literature. A continuous annual time-series of SSY was not possible at

426 the study site due to the discontinuous field campaigns and failure of or damage to the
427 turbidimeters during some months. Continuous records of P and Q were available for 2014, so
428 the Psum-SSY_{EV} and Qmax-SSY_{EV} models (Equation 5) were used to predict SSY_{EV} for all
429 storms in 2014 (Basher et al., 1997). Construction of sediment mitigation structures at the quarry
430 began in October 2014, greatly reducing SSY_{EV} from the LOWER_QUARRY subwatershed
431 (unpublished data), so the Qmax-SSY_{EV} relationship developed prior to the mitigation was used
432 to calculate the annual pre-mitigation sediment yield. For storms with no Qmax data at FG3,
433 Qmax was predicted from a linear regression between Qmax at FG1 and Qmax at FG3 for the
434 study period (R^2 =0.88).

435 Annual SSY and sSSY were also estimated by multiplying SSY_{EV} from measured storms
436 by the ratio of annual storm precipitation (P_{sann}) to the precipitation measured during storms
437 where SSY_{EV} was measured (P_{smeas}):

$$SSY_{ann} = SSY_{EV\_meas} * \frac{P_{EV\_ann}}{P_{EV\_meas}} \quad \text{Equation 6}$$

where SSY_{ann} is estimated annual SSY from storms, SSY_{EV_meas} is SSY_{EV} from sampled storms (all, Tables 2 and 4), P_{EV_meas} is precipitation measured during the sampled storms, and P_{EV_ann} is the precipitation during all storm events defined by the hydrograph separation.

438 Equation 6 assumes that the sediment yield per mm of storm precipitation is constant
439 over the year, and that the size distribution of storms has no effect on SSY_{EV}, though there is
440 some evidence that SSY_{EV} increases exponentially with storm size (Lewis et al., 2001; Rankl,
441 2004). Equation 6 also ignores sediment yield during non-storm periods, which is justified by the
442 low SSC and Q observed between storms.

Results

Field Data Collection

Precipitation

Annual precipitation measured at RG1, with gaps filled with data from Wx, was 3,502 mm, 3,529 mm, and 3,709 mm in 2012, 2013, and 2014, respectively, which averages 94% of long-term precipitation (=3,800 mm) from PRISM data (Craig, 2009). No difference in measured P was found between RG1 and Wx, or between RG1 and RG2, so P was assumed to be homogenous over the watershed for all analyses. Rain gauges could only be placed as high as ~300 m (RG2), though the highest point in the watershed is ~600 m. Long-term rain gage records show a strong precipitation gradient with increasing elevation, with average precipitation of 3,000-4,000 mm on the lowlands, increasing to more than 6,350 mm at high elevations (>400 m.a.s.l.) (Craig, 2009; Dames & Moore, 1981; Wong, 1996). Precipitation data measured at higher elevations would be useful to determine a more robust orographic precipitation relationship. For this analysis, however, the absolute values of total precipitation in each subwatershed are not as important since precipitation and the erosivity index are only used as predictive storm metrics.

Water Discharge

Discharge at both FG1 and FG3 was characterized by periods of low but perennial baseflow, punctuated by short, flashy hydrograph peaks (FG1: max 8,356 L/sec, FG3: max 13,071 L/sec) (Figure 3). Though Q data was unavailable for some periods, storm events were generally smaller but more frequent in the October-April wet season compared to the May-

September dry season. The largest event in the three year monitoring period was observed in the dry season (August 2014).

Storm Events

A total of 210 storm events were identified using hydrograph separation on the Q data at FG1 and FG3 between January, 2012, and December 2014. 169 events had simultaneous Q data at FG1 and FG3 (Appendix 3, Table 1). SSC data from T or interpolated grab samples were recorded during 112 events at FG1, and 74 events at FG3. Of those storms, 42 events had data for P, Q, and SSC at both FG1 and FG3 to calculate SSY_{EV} from the LOWER subwatershed. SSY data from interpolated grab samples were collected at FG2 for 8 storms to calculate SSY_{EV} from the LOWER_QUARRY and LOWER_VILLAGE subwatersheds separately. Storm event durations ranged from 1 hour to 2 days, with mean duration of 13 hours.

Most storm events showed a typical pattern, where a short period of intense rainfall caused a rapid increase in SSC downstream of the quarry (FG2) while SSC remained low at the undisturbed forest site (FG1) (Figure 4). The highest SSC was typically observed at FG2, with slightly lower and later peak SSC observed at FG3. SSC downstream of the undisturbed forest (FG1) typically increased more slowly, remained lower, and peaked later than the disturbed sites downstream of the quarry (FG2) and the village (FG3). Though peak SSC was highest at FG2, the highest SSY was measured at FG3 due to the addition of storm runoff and sediment from the larger subwatershed draining to FG3.

Suspended Sediment Concentration

From January 6, 2012, to October 1, 2014, 506 water samples were collected at FG1 (n=59), FG2 (n=90 grab samples, n=198 from the Autosampler), and FG3 (n=159). Mean (μ) and maximum SSC of water samples, collected during non-stormflow and stormflow periods by

487 grab and autosampler, were lowest at FG1 (μ=28 mg/L, max=500 mg/L), highest at FG2 (μ=337
488 mg/L, max=12,600 mg/L), and in between at FG3 (μ=148 mg/L, max=3,500 mg/L). At FG1,
489 24% of grab samples (n=14) were collected during non-stormflow, μ=8 mg/L (Figure 5a); 76%
490 of grab samples (n=45) were collected during stormflow, μ= 35 mg/L (Figure 8b). At FG2, 23%
491 of grab samples (n=21) were collected during non-stormflow, μ= 105 mg/L; 77% of grab
492 samples (n=69) were collected during stormflow, μ= 409 mg/L. At FG3, 25% of samples (n=39)
493 were collected during non-stormflow, μ= 52 mg/L; 75% of samples (n=120) were collected
494 during stormflow, μ= 179 mg/L. This pattern of SSC values suggests that little sediment is
495 contributed from the forest upstream of FG1, followed by a large input of sediment between FG1
496 and FG2, and then SSC is diluted by addition of stormflow with lower SSC between FG2 and
497 FG3.

498 Probability plots of the SSC data collected at FG1, FG2 and FG3 showed they were
499 highly non-normal, so non-parametric tests for statistical significance were applied. The results
500 of the Kruskall-Wallis test were significant for non-stormflow ($p<10^{-4}$) and stormflow ($p<10^{-4}$);
501 means of SSC samples were significantly different among all three locations. The results of the
502 pair-wise Mann-Whitney test between FG1 and FG2 were significant (non-stormflow, $p<10^{-4}$;
503 stormflow, $p<10^{-4}$), but between FG2 and FG3 were significant for non-stormflow ($p<0.05$) but
504 not for stormflow ($p>0.10$); means of SSC samples at FG1 and FG2 were significantly different,
505 but FG2 and FG3 were not.

506 SSC varied by several orders of magnitude for a given Q at FG1, FG2, and FG3 due to
507 significant hysteresis observed during storm periods (Figure 6). At FG1, variability of SSC
508 during stormflow was assumed to be caused by randomly occurring landslides or mobilization of
509 sediment stored in the watershed during large storm events. The maximum SSC sampled

510 downstream of the undisturbed forest, at FG1 (500 mg/L), was sampled on 04/23/2013 at high
511 discharge (QFG1= 3,724 L/sec) (Figure 6a). Anecdotal and field observations reported higher
512 than normal SSC upstream of the quarry during the 2013 field season, possibly due to landsliding
513 from previous large storms (G. Poysky, pers. comm.).

514 At FG2 and FG3, additional variability in the Q-SSC relationship was due to the
515 changing sediment availability associated with quarrying operations and construction in the
516 village. The high SSC values observed downstream of the quarry (FG2) during low Q were
517 caused by two mechanisms: 1) precipitation events that did not result in stormflow, but generated
518 runoff from the quarry with high SSC and 2) washing fine sediment into the stream during rock
519 crushing operations at the quarry.

520 The maximum SSC sampled at FG2 (12,600 mg/L) and FG3 (3,500 mg/L) were sampled
521 during the same rainfall event (03/05/2012), but during low Q (Q_FG3=287 L/sec) (Figure 6b-c).
522 During this event, brief but intense precipitation caused high sediment runoff from the quarry.
523 SSC was diluted further downstream of the quarry at FG3 by the addition of runoff with lower
524 SSC from the village.

525 Given the close proximity of the quarry to the stream, SSC downstream of the quarry can
526 be highly influenced by mining activity like rock extraction, crushing, and/or hauling operations.
527 During 2012, a common practice for removing fine sediment from crushed aggregate was to
528 rinse it with water pumped from the stream. In the absence of retention structures the fine
529 sediment was then discharged directly into the stream, causing high SSC during baseflow periods
530 with no precipitation in the preceding 24 hours (solid symbols, Figure 6b-c). Riverine discharge
531 of fine sediment rinsed from aggregate was discontinued in 2013. In 2013 and 2014, waste

sediment was piled on-site and severe erosion of these changing stockpiles caused high SSC during storm events.

Cumulative Probable Error (PE)

Cumulative Probable Error (RMSE %) for SSY_{EV} estimates at FG1 and FG3 were calculated from the measurement errors for Q (8.5%) and SSC grab samples (16.3%), and the model errors of the respective stage-Q and T-SSC relationships for that location. Cumulative Probable Errors (PE) in SSY_{EV} were 28-49% (μ=43%) at FG1 and 36-118% (μ=94%) at FG3.

The measurement error (RMSE) for Q at FG1 and FG3 was 8.5 %, which included error in the area-velocity measurements (6%), continuous Q measurement in a natural channel (6%), pressure transducer error (0.1%), and streambed condition (firm, stable bed=0%) (DUET-H/WQ look-up table (Harmel et al., 2006)). The model errors (RMSE) were 32% for the stage-Q rating curve using Manning's equation at FG3, and 22% using HEC-RAS at FG1.

The measurement error (RMSE) for SSC was 16.3%, which included errors for sample collection and analysis. Sample collection error consisted of interpolating over a 30 min interval (5%) and sampling during stormflows (3%). Sample analysis error was from measuring SSC by filtration (3.9%). The model errors (RMSE) of the T-SSC relationships were 16% (4 mg/L) for the YSI and TS turbidimeters at FG1, 113% (348 mg/L) for the YSI turbidimeter at FG3, and 46% (48 mg/L) for the OBS turbidimeter at FG3.

Comparing SSY_{EV} from disturbed and undisturbed subwatersheds

SSY_{EV} was measured simultaneously at FG1 and FG3 for 42 storms (Table 2). SSY_{EV_TOTAL} was 129.2±121.4 tons (72.6±68.2 tons/km²), with 17.0±7.3 tons (18.8±8.1 tons/km²) from the UPPER subwatershed and 112.2 tons (127.5 tons/km²) from the LOWER subwatershed. The UPPER and LOWER subwatersheds are similar in size (0.90 km² and 0.88

555 km²) but SSY_{EV_UPPER} accounted for an average of just 13% and SSY_{EV_LOWER} for 87% of SSY_{EV}
556 at the watershed outlet (Table 2). The DR estimated from $sSSY_{EV\_UPPER}$ (=18.8 tons/km²) and
557 $sSSY_{EV\_LOWER}$ (Equation 4) suggests $sSSY_{EV}$ has increased by 6.8x in the LOWER
558 subwatershed, and 3.9x for the TOTAL watershed.

559 SSY_{EV} from the undisturbed forest areas in the LOWER watershed was estimated to be
560 14.9 tons for the 42 events in Table 2 (Equation 3), so SSY_{EV} from the disturbed areas was 97.3
561 tons (Table 3). Approximately 87% of SSY_{EV_LOWER} was from disturbed areas, despite the
562 disturbed areas only accounting for 10.1% of the LOWER subwatershed area (0.089 km²).
563 Similarly, despite only 5.2% of the TOTAL watershed being disturbed, SSY from disturbed
564 areas accounted for 75% of SSY_{EV_TOTAL}. sSSY from disturbed areas in the LOWER
565 subwatershed was 1,095 tons/km², or 58x the sSSY of undisturbed forest.

566 It was hypothesized the quarry was a key sediment source, but SSY_{EV} was measured
567 simultaneously at FG1, FG2, and FG3 for only 8 of the storms in Table 2. SSY_{EV} was calculated
568 separately from the LOWER subwatershed containing the quarry ($SSY_{EV\_LOWER\_QUARRY}$) and
569 LOWER subwatershed containing the village below the quarry ($SSY_{EV\_LOWER\_VILLAGE}$) for those
570 8 storms (Table 4). For the 8 storms in Table 4, SSY_{EV_TOTAL} was 46 tons with an average of
571 29% from the UPPER subwatershed, 36% from the LOWER_QUARRY subwatershed, and 35%
572 from the LOWER_VILLAGE subwatershed. sSSY from the UPPER, LOWER_QUARRY, and
573 LOWER_VILLAGE subwatersheds, and the TOTAL watershed was 15, 61, 27, and 26 tons/km²,
574 respectively. The results from the smaller sample of storms in Table 4, show a slightly lower
575 increase in SSY from the TOTAL watershed, 1.7x, but show the sSSY has increased by 4.08x in
576 the LOWER_QUARRY subwatershed and 1.8x in the LOWER_VILLAGE subwatershed.

577 Very small fractions of the subwatershed areas are disturbed, yet roughly 77% of SSY
578 $_{EV\_LOWER\_QUARRY}$ (6.5% disturbed) and 51% of SSY $_{EV\_LOWER\_VILLAGE}$ (11.7% disturbed)
579 subwatersheds was from disturbed areas. Similarly, despite only 5.2% of the TOTAL watershed
580 being disturbed, 75-45% of SSY $_{EV\_TOTAL}$ was from disturbed areas (Tables 3 and 5). Bare land
581 in the LOWER_QUARRY subwatershed significantly increased $sSSY_{LOWER\_QUARRY}$ and
582 $sSSY_{TOTAL}$, and contributed the majority of SSY from disturbed areas in Faga'alu watershed.
583 sSSY from disturbed areas in the UPPER (37.0 tons/km²), LOWER_QUARRY (721.6 tons/km²),
584 and LOWER_VILLAGE subwatersheds (116.2 tons/km²) suggested that disturbed areas increase
585 sSSY over forested conditions by 49x and 8x in the LOWER_QUARRY and
586 LOWER_VILLAGE subwatersheds, respectively. Human disturbance in the
587 LOWER_VILLAGE subwatershed also increased SSY above natural levels but the magnitude of
588 disturbance was much lower than the quarry.

589 ## Predicting SSY_{EV} from storm metrics

590 SSY_{EV} from the UPPER and TOTAL watersheds was correlated with each of the four
591 storm metrics tested (Figure 7), though the correlations with precipitation metrics were poor in
592 the heavily forested UPPER watershed (Table 6). Pearson and Spearman correlation coefficients
593 were similar, meaning the relationships were mostly linear in log-log space. Significant scatter
594 was observed around all models, which reflects the changing sediment availability at the quarry
595 and village, and the natural variability in the watershed response for different storm events.
596 Qsum was the best predictor of SSY_{EV} for the UPPER watershed, and Psum was the best
597 predictor for the TOTAL watershed, though Qmax was nearly as good a predictor for both
598 watersheds. SSY_{EV} is calculated from Q so it is expected that Qsum should correlate closely with
599 SSY_{EV}, as observed in other studies (Duvert et al., 2012; Rankl, 2004). Indeed the Qsum model

600 for the UPPER watershed showed the highest coefficient of determination (r^2), lowest RMSE,
601 and highest Pearson and Spearman correlation coefficients (Table 6). Psum showed an equally
602 high r^2 and a lower RMSE, but only for the TOTAL subwatershed. This suggests that sediment
603 production is more related to discharge processes in the UPPER subwatershed, and more related
604 to precipitation processes in the LOWER subwatershed. Discharge metrics were also highly
605 correlated with SSY_{EV} in the TOTAL watershed, suggesting discharge metrics are good
606 predictors in both disturbed and undisturbed watersheds. Qmax was not the best predictor in
607 either watershed, but performed well in both watersheds, with similar correlation statistics to
608 both Qsum and Psum models. Most of the scatter in the Qmax-SSY_{EV} relationship is observed
609 for small events, and Qmax correlated strongly with the largest SSY_{EV} values when most of the
610 annual sediment load is generated.
611 Precipitation was measured at the quarry, which may reflect precipitation characteristics
612 more accurately in the LOWER than the UPPER watershed. SSY from the LOWER
613 subwatershed is hypothesized to be mostly generated by hillslope erosion by sheetwash and rill
614 formation at the quarry and on dirt roads, and agricultural plots, whereas SSY from the UPPER
615 subwatershed is hypothesized to be mainly from channel processes and mass wasting. Mass
616 wasting can contribute large pulses of sediment which can be deposited near or in the streams
617 and entrained at high discharges during later storm events. Given the high correlation
618 coefficients between SSY_{EV} and Qmax in both watersheds, Qmax may be a promising predictor
619 that integrates both precipitation and discharge processes.
620 In all models, SSY_{EV} from the TOTAL watershed was higher than from the UPPER
621 watershed for the full range of measured storms with the exception of a few events that are
622 considered outliers. These events could be attributed to measurement error or to landslides in the

623 UPPER subwatershed and the increased sediment supply for that specific event. The separation
624 of multi-peak storm events, storm sequence, and antecedent conditions may also play a role.
625 While the climate on Tutuila is tropical, without strong seasonality, periods of low rainfall can
626 persist for several weeks, perhaps altering the water and sediment dynamics in the subsequent
627 storm events.

628 All model intercepts (α) were significantly different ($p<0.01$), but only the Qsum-SSY_{EV}
629 model showed significantly different ($p<0.01$) slopes (β). The Qsum-SSY_{EV} models indicate that
630 SSY_{EV} from the UPPER and TOTAL watersheds converge at higher Qsum values. Conversely,
631 the Psum- and Qmax-SSY_{EV} models show no change in relative contributions of SSY over the
632 range of storm sizes (Figure 7).

633 The relative contribution from the human-disturbed watershed was hypothesized to
634 diminish with increasing storm size. The results from precipitation metrics and discharge metrics
635 were contradictory. The relative contribution of SSY_{EV} from the human-disturbed watershed
636 decreases with storm size in the Qsum-SSY_{EV} model, but the Psum- and Qmax-SSY_{EV} models
637 show no change in relative contributions over increasing storm size (Figure 7). It was
638 hypothesized that SSY_{EV} from natural areas would become the dominant source for larger storm
639 events, but the DR remains high for large storm events due to the naturally low SSY_{EV} from
640 natural forest areas in Faga'alu watershed. This suggests that disturbed areas were not supply
641 limited for the range of sampled storms.

642 ## Annual estimates of SSY and sSSY

643 Estimates of annual sSSY depended on which predictor was used to estimate SSY_{EV}.
644 Annual sSSY from the UPPER and TOTAL watersheds was 14 tons/km²/yr and 75 tons/km²/yr,
645 respectively, as predicted by Psum-SSY_{EV} relationship, and 68 tons/km²/yr and 247 tons/km²/yr,

646 respectively using the Qmax-SSY_{EV} relationship (Table 7). The large difference in sSSY
647 between the two methods was due to higher scatter about the Psum-SSY_{EV} relationship for large
648 events compared with the Qmax-SSY_{EV}. These results suggest the UPPER watershed contributed
649 14%, and the LOWER subwatershed contributed 86% of annual SSY from the TOTAL
650 watershed.

651 In order to compare with SSY estimated from the Psum-SSY_{EV} and Qmax-SSY_{EV}
652 relationships, annual SSY was also calculated using Equation 6 for three sets of storm events: a)
653 all events with SSY_{EV} data, including those where SSY_{EV} data were only available for a single
654 site; b) only events where data was available for both UPPER (FG1) and TOTAL (FG3) and c)
655 only events where data was available for UPPER (FG1), LOWER_QUARRY (FG2), and
656 TOTAL (FG3). Including all storms (method a) will provide the best estimate at a given location,
657 while b) and c) allow more direct comparison of different subwatersheds. Continuous records of
658 Q and precipitation in 2014 showed annual storm precipitation (P_{sann}) was 2,770 mm,
659 representing 69% of total annual precipitation (3,709 mm). All storms with measured SSY_{EV} at
660 FG1 from 2012-2014 included 3,457 mm of precipitation (P_{smeas}), or 125% of P_{sann}, so estimated
661 annual SSY from the UPPER subwatershed from Equation 6 was 41 tons/yr (45 tons/km²/yr). All
662 storms with measured SSY_{EV} at FG3 from 2012-2014 included 2,628 mm of precipitation, or
663 95% of expected annual storm precipitation so estimated annual SSY from the TOTAL
664 watershed was 428 tons/yr (241 tons/km²/yr). These results suggest the UPPER watershed
665 contributed 10%, and the LOWER subwatershed contributed 90% of annual SSY from the
666 TOTAL watershed.

667 For storms with measured SSY_{EV} at both FG1 and FG3 (Table 2), P_{EVmeas} was 1,004 mm,
668 or 36% of P_{EVann}. From Equation 6, annual SSY increased from the UPPER (46 tons/yr),

669 LOWER (310 tons/yr), and TOTAL watershed (360 tons/yr). Annual sSSY increased from the
670 UPPER (51 tons/km^2/yr), LOWER (350 tons/km^2/yr), and TOTAL watershed (200 tons/km^2/yr),
671 and, respectively.

672 For storms with measured SSY_{EV} at FG1, FG2, and FG3 (Table 4), P_{EVmeas} was 299 mm,
673 or 11% of P_{EVann}. Annual SSY increased from the UPPER (120 tons/yr), LOWER_QUARRY
674 subwatershed (150 tons/yr), LOWER_VILLAGE subwatershed (150 tons/yr), LOWER
675 subwatershed (300 tons/yr), and TOTAL watershed (420 tons/yr). Annual sSSY increased from
676 the UPPER (140 tons/km^2/yr), LOWER_QUARRY (560 tons/km^2/yr), LOWER_VILLAGE (250
677 tons/km^2/yr), LOWER (340 tons/km^2/yr), and TOTAL watershed 240 tons/km^2/yr.

678 Overall, the Qmax model and Equation 6 using all events gave similar estimates of
679 annual SSY at both the UPPER watershed (41-61 tons/yr) and the total watershed (428-439
680 tons/yr). The accuracy of the Psum model was compromised by significant scatter for large
681 events, while the Qsum model had significantly less scatter for large events. The eight storms
682 sampled at all three locations (Table 4) had unusually high loads from the upper watershed but
683 similar SSY from the lower watershed, likely resulting in a low estimate of sediment loading and
684 DR from the quarry.

685 ## Discussion

686 ### Methods for quantifying human impact

687 Event-wise measurement of SSY_{EV} allowed rapid quantification of sediment loading
688 from natural and human-disturbed areas. Event wise analysis was useful because hysteresis and
689 interstorm variability caused significant scatter in the instantaneous Q-SSC relationship. While
690 the instantaneous Q-SSC relationship illustrated large increases in SSC downstream of the

691 quarry, the hysteresis and interstorm variability meant that a single Q-SSC relationship could not
692 be used to estimate of sediment loading, which complicated detection of human impact on
693 sediment concentrations and yield. Measurement of SSY_{EV} allows comparison of similar size
694 storms to determine change over space and time without problems of interannual variability in
695 precipitation totals, and the simple regression models that predict annual sediment load from
696 either precipitation or stormflow measurements eliminate the need for long-term field work to
697 estimate annual total yields. From a management perspective, the event-wise approach to
698 estimating human impacts on sediment is less expensive than efforts to measure annual yields
699 since it does not require a full year of monitoring and can be rapidly conducted if mitigation or
700 disturbance activities are already planned. With predictive models of SSY_{EV} that are based on an
701 easily-monitored storm metric like maximum event discharge, SSY_{EV} can be modeled in the
702 future to compare with either post-mitigation or post-disturbance SSY_{EV}.

703 The estimation of human impact on sediment loads was facilitated by the spatial
704 arrangement of disturbances and by the lack of significant sediment storage in the watershed. In
705 Faga'alu watershed, and other similar steep watersheds, human-disturbance is often constrained
706 to the lower watershed, and sediment yields from these key sources can be measured separately
707 from the undisturbed forest upstream. Reid and Dunne (1996) argue that in cases where there is a
708 clear management question and the study area can be divided into sub-units, a sediment budget
709 can be rapidly developed with only a few field measurements and limited periods of field
710 monitoring. The use of event-wise sampling in subwatersheds with specific land uses allowed for
711 separation of different sources to the sediment budget.

Interpreting slope and intercept of the Qmax-SSY_{EV} relationship

Several researchers have attempted to explain values of the intercept (α) and slope (β) coefficients of the sediment rating curve as a function of watershed characteristics. A traditional sediment rating curve (Q-SSC) is considered a 'black box' model, and though the slope and intercept have no physical meaning, some physical interpretation has been ascribed to them (Asselman, 2000). Rankl (2004) hypothesized that the intercept in the Qmax-SSY_{EV} relationship varied with sediment availability and erodibility in watersheds. Duvert et al. (2012) found that intercepts of the Qmax-SSY_{EV} relationship are also dependent on the regression fitting method. While slopes in log-log space can be compared directly (Duvert et al., 2012), intercepts must be plotted in similar units, and normalized by watershed area. In five semi-arid to arid watersheds (2.1-1,538 km²) in Wyoming, United States (Rankl, 2004), intercepts of the SSY_{EV}-Qmax relationship ranged from 111-4,320 (Qmax in m³/s/km², SSY_{EV} in Mg/km²). In eight sub-humid to semi-arid watersheds (0.45-22 km²) (Duvert et al., 2012), the intercepts ranged from 25-5,039. In Faga'alu, the intercept in the undisturbed, UPPER subwatershed was 0.35, and in the disturbed, TOTAL watershed the intercept was 1.38, which are an order of magnitude or two lower than the lowest intercepts in Rankl (2004) and Duvert et al. (2012). This suggests that sediment availability is relatively low in Faga'alu, under natural and human-disturbed conditions, likely due to the dense forest cover.

High slope values in the log-log plots (β coefficient) suggest that small changes in stream discharge lead to large increases in sediment load due to the erosive power of the river or the availability of new sediment sources at high Q (Asselman, 2000). Rankl (2004) assumed that the slope was a function of rainfall intensity on hillslopes, and found that the slopes ranged from 1.07-1.29 in five semi-arid to arid watersheds in Wyoming, and were not statistically different

among watersheds. In the watersheds in Duvert et al. (2012), slopes ranged from 0.95-1.82, and from 1.06-2.45 in eighteen other watersheds (0.60-1,538 km²) in diverse geographical settings (Basher et al., 1997; Fahey and Marden, 2000; Hicks et al., 2009; Rankl, 2004; Tropeano, 1991) compiled by Duvert et al. (2012). In Faga'alu, slopes were 1.51 and 1.40 in the UPPER and TOTAL Faga'alu watersheds, respectively, which are very consistent with the slopes presented in Rankl (2004) and Duvert et al. (2012), despite large differences in climate and land cover.

In Faga'alu, SSY_{EV} was least correlated with the Erosivity Index (EI30). Duvert et al. (2012) also found low correlation coefficients with 5 min rainfall intensity for 8 watersheds in France and Mexico. Rodrigues et al. (2013) hypothesized that EI30 is poorly correlated with SSY_{EV} due to the effect of previous events on antecedent moisture conditions and in-channel sediment storage. Cox et al. (2006) found EI30 was more correlated with soil loss in an agricultural watershed than a forested watershed, and Faga'alu is mainly covered in dense forest. Similar to other studies (Basher et al., 2011; Duvert et al., 2012; Fahey et al., 2003; Hicks, 1990; Rankl, 2004; Rodrigues et al., 2013) the highest correlations with SSY_{EV} at Faga'alu were observed for discharge metrics. While Qsum and Psum had higher correlations in individual watersheds, Qmax was a good predictor of SSY_{EV} in both the disturbed and undisturbed watershed.

Comparing sSSY and SSC in other small Pacific Island watersheds

Sediment yield is highly variable among individual watersheds, but is generally controlled by climate, vegetation cover, and geology, with human disturbance playing an increasing role in the 20th century (Syvitski et al., 2005). Sediment yields in tropical Southeast Asia and high-standing islands between Asia and Australia range from ~10 tons/km²/yr in the granitic Malaysian Peninsula to ~10,000 tons/km²/yr in the tectonically active, steeply sloped

758 island of Papua New Guinea (Douglas, 1996). Sediment yields from Faga'alu are on the lower
759 end of the range, with sSSY of 45-68 tons/km²/yr from the undisturbed UPPER watershed, and
760 241-247 tons/km²/yr from the disturbed TOTAL watershed.

761 Milliman and Syvitski (1992) report high average sSSY (1,000-3,000 tons/km²/yr) from
762 watersheds (10-100,000 km²) in tropical Asia and Oceania, though their regional models of sSSY
763 as a function of basin size and maximum elevation predict only 13 tons/km²/yr from watersheds
764 with peak elevation 500-1,000 m (highest point of UPPER Faga'alu subwatershed is 653 m), and
765 68 tons/km²/yr for max elevations of 1,000-3,000. Given the high vegetation cover and lack of
766 human activity in the UPPER Faga'alu subwatershed, its sSSY should be lower than sSSY from
767 watersheds presented in Milliman and Syvitski (1992), which included watersheds with human
768 disturbance. sSSY from the forested UPPER Faga'alu subwatershed (45-68 tons/km²/yr) was
769 approximately three to five times higher than the prediction from the Milliman and Syvitski
770 (1992) model (13 tons/km²/yr). The scatter around their model is large for smaller watersheds,
771 and the Faga'alu data fall within the range of scatter (Figures 5e and 6e in Milliman and Syvitski
772 (1992)).

773 Sediment yield has been measured using modern fluvial measurements similar to ours for
774 two Hawaiian watersheds: Hanalei watershed on Kauai ("Hanalei"), and Kawela watershed on
775 Molokai ("Kawela") (Table 8) (Ferrier et al., 2013; Stock and Tribble, 2010). Hanalei (54 km²)
776 has steep relief and mean areal precipitation of 3,866 mm/yr (Ferrier et al., 2013), which is
777 slightly higher than rainfall at Faga'alu during the observation period (3,247 mm/yr). Over a four
778 year period, SSC at Hanalei averaged 63 mg/L and reached a maximum of 2,750 mg/L (Stock
779 and Tribble, 2010), which is slightly lower than observations at Faga'alu (mean 148 mg/L,
780 maximum 3,500 mg/L). Calhoun and Fletcher (1999) estimated sSSY from Hanalei as 140±55

781 tons/km²/yr, but had fewer data than Stock and Tribble (2010), who estimated sSSY as 525
782 tons/km²/yr. Ferrier et al., (2013) reported annual suspended sediment yield at Hanalei as 369 ±
783 114 tons/km^2/yr. These values are all higher than observed at Faga'alu under both undisturbed
784 (45-68 tons/km^2/yr) and disturbed (430-441 tons/km^2/yr) subwatersheds. Rocks at Hanalei are of
785 similar age (1.5 Mya) or older (3.95-4.43 Mya) (Ferrier et al., 2013) compared with Faga'alu
786 (1.2 Mya) (McDougall, 1985), so landscape age does not explain the difference in observed SSY
787 between Hanalei and Faga'alu. Kawela (14 km²) is disturbed by grazing and is in a sub-humid
788 climate, where precipitation varies with elevation from 500-3,000 mm. Stock and Tribble (2010)
789 estimated sSSY from Kawela as 459 tons/km²/yr, which is similar to the disturbed subwatershed
790 in Faga'alu, but nearly twice as high as the TOTAL Faga'alu watershed. In Kawela, SSC (mean
791 3,490 mg/L, maximum 54,000 mg/L) was much higher than measured in Faga'alu TOTAL
792 watershed, so the difference in SSY is due in part to higher SSC rather than to higher observed
793 runoff. Overall, both Hawaiian watersheds have higher SSY than Faga'alu, which is consistent
794 with the low intercepts of Faga'alu in the Qmax-SSY_{EV} relationships, and suggests that Faga'alu
795 may have uniquely low erosion rates for a steep volcanic watershed. Precipitation variability may
796 contribute to the difference in SSY, so a more thorough comparison between Hanalei and
797 Faga'alu would require a storm-wise analysis of the type performed here.
798 Annual sSSY from the quarry was estimated from Equation 6 to be approximately 2,800
799 tons/km²/yr. The quarry surfaces are comprised of haul roads, piles of overburden, and steep rock
800 faces which can be described as a mix of unpaved roads and cut-slopes. Literature values show
801 measured sSSY from cutslopes varying from 0.01 tons/km²/yr in Idaho (Megahan, 1980) to
802 105,000 tons/km²/yr in Papua New Guinea (Blong and Humphreys, 1982), so the sSSY ranges
803 measured in this study are well within the ranges found in the literature.

Comparison with other kinds of sediment disturbance

Other studies in small, mountainous watersheds have documented one to several orders of magnitude increases in SSY from land use that disturbs a small fraction of the watershed area. Urbanization and mining can increase sediment yield by two to three orders of magnitudes in catchments of several km². Yields from construction sites can exceed those from the most unstable, tectonically active natural environments of Southeast Asia (Douglas, 1996). In Kawela watershed on Molokai, less than 5% of the land produces most of the sediment, and only 1% produces ~50% of the sediment (Risk, 2014; Stock et al., 2010). In three basins on St. John, US Virgin Islands unpaved roads increased sediment delivery rates by 3-9 times (Ramos-Scharrón and Macdonald, 2005). Disturbances at larger scales have resulted in similar increases in total SSY to coral environments. The development of the Great Barrier Reef (GBR) catchment (423,000 km^2) since European settlement (ca.1830) led to increases in SSY by an estimated factor of 5.5x (Kroon et al., 2012). Mining has been a major contributor of sediment in other watersheds on volcanic islands with steep topography and high precipitation, increasing sediment yields by 5-10 times in a watershed in Papua New Guinea (Hettler et al., 1997; Thomas et al., 2003). In contrast to other land disturbances like fire, logging, or urbanization where sediment disturbance decreases over time, the disturbance from mining is persistently high. Disturbance magnitudes are similar to the construction phase of urbanization (Wolman and Schick, 1967), or high-traffic unpaved roads (Reid and Dunne, 1984), but persist or even increase over time.

While unpaved roads are often identified as a source of sediment in humid forested regions (Lewis et al., 2001; Ramos-Scharrón and Macdonald, 2005; Reid and Dunne, 1984), field observations at Faga'alu suggested that most roads in the urban area were stabilized with aggregate and not generating significant amounts of sediment. Other disturbances in Faga'alu

included a few small agricultural plots, small construction sites and bare dirt on roadsides. Repeated surface disturbance at the quarry is a key process maintaining high rates of sediment generation. Given the large distance to other sources of building material, aggregate mining and associated sediment disturbance may be a critical sediment source on remote islands in the Pacific and elsewhere.

Conclusion

Human disturbance has increased sediment yield to Faga'alu Bay by 3.9x over pre-disturbance levels. The human-disturbed subwatershed accounted for the majority (87%) of total sediment yield, and the quarry (1.1% of watershed area) contributed about a third of total SSY to the Bay. Qmax was a good predictor of SSY_{EV} in both the disturbed and undisturbed watershed, making it a promising predictor in diverse environments. The slopes of the Qmax-SSY_{EV} relationships were comparable with other studies, but the model intercepts were an order of magnitude lower than intercepts from watersheds in semi-arid to semi-humid climates. This suggests that sediment availability is relatively low in the Faga'alu watershed, either because of the heavy forest cover or volcanic rock type. The event-wise approach did not require continuous in situ monitoring for a single or multiple years, which would not have been logistically possible in this remote study area. This study presents an innovative method to combine sampling and analysis strategies to measure sediment contributions from key sources, estimate baseline annual sediment yields prior to management, and rapidly develop an empirical sediment yield model for a remote, data-poor watershed.

Acknowledgements

Funding for this project was provided by NOAA Coral Reef Conservation Program (CRCP) through the American Samoa Coral Reef Advisory Group (CRAG). Kristine Bucchianeri at CRAG and Susie Holst at NOAA CRCP provided necessary and significant support. Christianera Tuitele, Phil Wiles, and Tim Bodell at American Samoa Environmental Protection Agency (ASEPA), and Fatima Sauafea-Leau and Hideyo Hattori at NOAA, provided on-island coordination with traditional local authorities. Dr. Mike Favazza provided critical logistical assistance in American Samoa. Robert Koch at the American Samoa Coastal Zone Management Program (ASCMP) and Travis Bock at ASEPA assisted in accessing historical geospatial and water quality data. Many others helped and supported the field and laboratory work including Professor Jameson Newtson, Rocco Tinitali, and Valentine Vaeoso at American Samoa Community College (ASCC), Meagan Curtis and Domingo Ochavillo at American Samoa Department of Marine and Wildlife Resources (DMWR), Don and Agnes Vargo at American Samoa Land Grant, Christina Hammock at NOAA American Samoa Climate Observatory, and Greg McCormick at San Diego State University. George Poysky, Jr., George Poysky III, and Mitch Shimisaki at Samoa Maritime Ltd. provided unrestricted access to the Faga'alu quarry site, and historical operation information. Faafetai tele lava.

References

Asselman, N.E.M., 2000. Fitting and interpretation of sediment rating curves. J. Hydrol. 234, 228–248. doi:10.1016/S0022-1694(00)00253-5

867 Basher, L., Hicks, D., Clapp, B., Hewitt, T., 2011. Sediment yield response to large storm events
868 and forest harvesting, Motueka River, New Zealand. New Zeal. J. Mar. Freshw. Res. 45,
869 333–356. doi:10.1080/00288330.2011.570350

870 Basher, L.R., Hicks, D.M., Handyside, B., Ross, C.W., 1997. Erosion and sediment transport
871 from the market gardening lands at Pukekohe, Auckland, New Zealand. J. Hydrol. 36, 73–
872 95.

873 Bégin, C., Brooks, G., Larson, R. a., Dragićević, S., Ramos Scharrón, C.E., Coté, I.M., 2014.
874 Increased sediment loads over coral reefs in Saint Lucia in relation to land use change in
875 contributing watersheds. Ocean Coast. Manag. 95, 35–45.
876 doi:10.1016/j.ocecoaman.2014.03.018

877 Blong, R.J., Humphreys, G.S., 1982. Erosion of road batters in Chim Shale, Papua New Guinea.
878 Civ. Eng. Trans. Inst. Eng. Aust. CE24 1, 62–68.

879 Bonta, J. V, 2000. Impact of Coal Surface Mining and Reclamation on Suspended Sediment in
880 Three Ohio Watersheds. JAWRA J. Am. Water Resour. Assoc. 36, 869–887.

881 Brunner, G., 2010. HEC-RAS River Analysis System.

882 Buchanan-Banks, J., 1979. The October 28, 1979 Landslidng on Tutuila. Open File Report 81-
883 81. U.S. Geological Survey.

884 Calhoun, R.S., Fletcher, C.H., 1999. Measured and predicted sediment yield from a subtropical,
885 heavy rainfall, steep-sided river basin: Hanalei, Kauai, Hawaiian Islands. Geomorphology
886 30, 213–226.

887 Cox, C.A., Sarangi, A., Madramootoo, C.A., 2006. Effect of land management on runoff and soil
888 losses from two small watersheds in St Lucia. L. Degrad. Dev. 17, 55–72.
889 doi:10.1002/ldr.694

890 Craig, P., 2009. Natural History Guide to American Samoa. National Park of American Samoa,
891 Pago Pago, American Samoa.

892 Curtis, S., Wetzell, L., Wiles, P., Tinitali, R., 2011. Turbidity in Faga'alu Stream: The Sources,
893 Impacts, and Solutions.

894 Daly, C., Halbleib, M., Smith, J.I., Gibson, W.P., Doggett, M.K., Taylor, G.H., Curtis, J.,
895 Passteris, P.P., 2008. Physiographically sensitive mapping of climatological temperature
896 and precipitation across the conterminous United States. Int. J. Climatol. 28, 2031.
897 doi:10.1002/joc

898 Dames & Moore, 1981. Hydrologic Investigation of Surface Water for Water Supply and
899 Hydropower.

900 Douglas, I., 1996. The impact of land-use changes, especially logging, shifting cultivation,
901 mining and urbanization on sediment yields in humid tropical Southeast Asia: A review
902 with special reference to Borneo. IAHS-AISH Publ. 236, 463–471.

903 Dunne, T., Leopold, L.B., 1978. Water in environmental planning. W.H. Freeman and Company,
904 New York.

905 Duvert, C., Gratiot, N., 2010. Construction of the stage-discharge rating curve and the SSC-
906 turbidity calibration curve in San Antonio Coapa 2009 hydrological season.

907 Duvert, C., Nord, G., Gratiot, N., Navratil, O., Nadal-Romero, E., Mathys, N., Némery, J.,
908 Regüés, D., García-Ruiz, J.M., Gallart, F., Esteves, M., 2012. Towards prediction of
909 suspended sediment yield from peak discharge in small erodible mountainous catchments
910 (0.45–22km2) of France, Mexico and Spain. J. Hydrol. 454-455, 42–55.
911 doi:10.1016/j.jhydrol.2012.05.048

912 Eyre, P.R., 1989. Ground-water quality reconnaissance, Tutuila, American Samoa, U.S.
913 Geological Survey Water Resources Investigations Report 94-4142. Honolulu, HI.

914 Fabricius, K.E., 2005. Effects of terrestrial runoff on the ecology of corals and coral reefs:
915 review and synthesis. Mar. Pollut. Bull. 50, 125–46. doi:10.1016/j.marpolbul.2004.11.028

916 Fahey, B.D., Marden, M., 2000. Sediment yields from a forested and a pasture catchment,
917 coastal Hawke's Bay, North Island, New Zealand. J. Hydrol. 39, 49–63.

918 Fahey, B.D., Marden, M., Phillips, C.J., 2003. Sediment yields from plantation forestry and
919 pastoral farming, coastal Hawke's Bay, North Island, New Zealand. J. Hydrol. 42, 27–38.

920 Fenner, D., Speicher, M., Gulick, S., Aeby, G., Aletto, S.C., Anderson, P., Carroll, B.P.,
921 DiDonato, E.M., DiDonato, G.T., Farmer, V., Fenner, D., Gove, J., Gulick, S., Houk, P.,

922 Lundblad, E., Nadon, M., Riolo, F., Sabater, M.G., Schroeder, R., Smith, E., Speicher, M.,
923 Tuitele, C., Tagarino, A., Vaitautolu, S., Vaoli, E., Vargas-angel, B., Vroom, P., 2008. The
924 State of Coral Reef Ecosystems of American Samoa, in: The State of Coral Reef
925 Ecosystems of the United States and Pacific Freely Associated States. pp. 307–351.

926 Ferrier, K.L., Taylor Perron, J., Mukhopadhyay, S., Rosener, M., Stock, J.D., Huppert, K.L.,
927 Slosberg, M., 2013. Covariation of climate and long-term erosion rates across a steep
928 rainfall gradient on the Hawaiian island of Kaua'i. Bull. Geol. Soc. Am. 125, 1146–1163.
929 doi:10.1130/B30726.1

930 Fuka, D., Walter, M., Archibald, J., Steenhuis, T., Easton, Z., 2014. EcoHydRology.

931 Gellis, A.C., 2013. Factors influencing storm-generated suspended-sediment concentrations and
932 loads in four basins of contrasting land use, humid-tropical Puerto Rico. Catena 104, 39–57.
933 doi:10.1016/j.catena.2012.10.018

934 Gippel, C.J., 1995. Potential of turbidity monitoring for measuring the transport of suspended
935 solids in streams. Hydrol. Process. 9, 83–97.

936 Gomi, T., Moore, R.D., Hassan, M.A., 2005. Suspended sediment dynamics in small forest
937 streams of the Pacific Northwest. J. Am. Water Resour. Assoc.

938 Gray, J.R., 2014. Measuring Suspended Sediment, in: Ahuja, S. (Ed.), Comprehensive Water
939 Quality and Purification. Elsevier, pp. 157–204. doi:10.1016/B978-0-12-382182-9.00012-8

940 Gray, J.R., Glysson, G.D., Turcios, L.M., Schwarz, G.E., 2000. Comparability of Suspended-
941 Sediment Concentration and Total Suspended Solids Data U.S. Geological Survey Water-
942 Resources Investigations Report 00-4191. Reston, Va.

943 Harmel, R.D., Cooper, R.J., Slade, R.M., Haney, R.L., Arnold, J.G., 2006. Cumulative
944 uncertainty in measured streamflow and water quality data for small watersheds. Trans.
945 Am. Soc. Agric. Biol. Eng. 49, 689–701.

946 Harmel, R.D., Smith, D.R., King, K.W., Slade, R.M., 2009. Estimating storm discharge and
947 water quality data uncertainty: A software tool for monitoring and modeling applications.
948 Environ. Model. Softw. 24, 832–842.

949 Harrelson, C.C., Rawlins, C.L., Potyondy, J.P., 1994. Stream channel reference sites: an
950 illustrated guide to field technique. USDA Forest Service General Technical Report RM-
951 245. US Department of Agriculture, Fort Collins, CO.

952 Henderson, G.W., Toews, D.A.A., 2001. Using Sediment Budgets to Test the Watershed
953 Assessment Procedure in Southeastern British Columbia, in: Toews, D.A.A., Chatwin, S.
954 (Eds.), Watershed Assessment in the Southern Interior of British Columbia. B.C. Ministry
955 of Forests, Research Branch, Victoria, British Columbia, pp. 189–208.

956 Hettler, J., Irion, G., Lehmann, B., 1997. Environmental impact of mining waste disposal on a
957 tropical lowland river system: a case study on the Ok Tedi Mine, Papua New Guinea.
958 Miner. Depos. 32, 280–291. doi:10.1007/s001260050093

959 Hicks, D.M., 1990. Suspended sediment yields from pasture and exotic forest basins, in:
960 Proceedings of the New-Zealand Hydrological Society Symposium. Auckland, New
961 Zealand.

962 Hicks, D.M., Hoyle, J., Roulston, H., 2009. Analysis of sediment yields within Auckland region.
963 ARC Technical Report 2009/064. Prepared by NIWA for Auckland Regional Council.

964 Holst-Rice, S., Messina, A., Biggs, T.W., Vargas-Angel, B., Whitall, D., 2015. Baseline
965 Assessment of Faga'alu Watershed: A Ridge to Reef Assessment in Support of Sediment
966 Reduction Activities. NOAA Coral Reef Conservation Program, Silver Spring, MD.

967 Horsley-Witten, 2011. American Samoa Erosion and Sediment Control Field Guide.

968 Horsley-Witten, 2012. Post-Construction Stormwater Training Memorandum.

969 Izuka, S.K., Giambelluca, T.W., Nullet, M.A., 2005. Potential Evapotranspiration on Tutuila ,
970 American Samoa. U.S. Geological Survey Scientific Investigations Report 2005-5200.

971 Kearns, R., 2013. Personal Communication.

972 Kinnell, P.I.A., 2013. Modelling event soil losses using the Q R EI 30 index within RUSLE2.
973 Hydrol. Process. doi:10.1002/hyp

974 Kroon, F.J., Kuhnert, P.M., Henderson, B.L., Wilkinson, S.N., Kinsey-Henderson, A., Abbott,
975 B., Brodie, J.E., Turner, R.D.R., 2012. River loads of suspended solids, nitrogen,
976 phosphorus and herbicides delivered to the Great Barrier Reef lagoon. Mar. Pollut. Bull. 65,
977 167–81. doi:10.1016/j.marpolbul.2011.10.018

978 Latinis, D.K., Moore, J., Kennedy, J., 1996. Archaeological Survey and Investigations
979 Conducted at the Faga'alu Quarry, Ma'oputasi County, Tutuila, American Samoa, February
980 1996: Prepared for George Poysky, Sr., Samoa Maritime, PO Box 418, Pago Pago,
981 American Samoa, 96799. Archaeological Consultants of the Pacific Inc., 59-624 Pupukea
982 Rd., Haleiwa, HI 96712.

983 Lewis, J., 1996. Turbidity-controlled suspended sediment sampling for runoff-event load
984 estimation. Water Resour. Res. 32, 2299–2310.

985 Lewis, J., Mori, S.R., Keppeler, E.T., Ziemer, R.R., 2001. Impacts of Logging on Storm Peak
986 Flows , Flow Volumes and Suspended Sediment Loads in Caspar Creek, CA, in: Land Use
987 and Watersheds: Human Influence on Hydrology and Geomorphology in Urban and Forest
988 Areas. pp. 1–76.

989 McDougall, I., 1985. Age and Evolution of the Volcanoes of Tutuila American Samoa. Pacific
990 Sci. 39, 311–320.

991 Megahan, W.F., 1980. Erosion from roadcuts in granitic slopes of the Idaho Batholith, in:
992 Proceedings Cordilleran Sections of the Geological Society of America, 76th Annual
993 Meeting. Oregon State University, Corvallis, OR, p. 120.

994 Megahan, W.F., Wilson, M., Monsen, S.B., 2001. Sediment production from granitic cutslopes
995 on forest roads in Idaho, USA. Earth Surf. Process. Landforms 26, 153–163.

996 Menking, J. a., Han, J., Gasparini, N.M., Johnson, J.P.L., 2013. The effects of precipitation
997 gradients on river profile evolution on the Big Island of Hawai'i. Bull. Geol. Soc. Am. 125,
998 594–608. doi:10.1130/B30625.1

999 Milliman, J.D., Syvitski, J.P.M., 1992. Geomorphic/tectonic control of sediment discharge to the
1000 ocean: the importance of small mountainous rivers. J. Geol. 100, 525–544.

1001 Nakamura, S., 1984. Soil Survey of American Samoa. US Department of Agriculture Soil
1002 Conservation Service, Pago Pago, American Samoa.

1003 Nathan, R.J., McMahon, T. a, 1990. Evaluation of Automated Techniques for Base Flow and
1004 Recession Analyses. Water Resour. Res. 26, 1465–1473. doi:10.1029/WR026i007p01465

1005 Nearing, M. a, Nichols, M.H., Stone, J.J., Renard, K.G., Simanton, J.R., 2007. Sediment yields
1006 from unit-source semiarid watersheds at Walnut Gulch. Water Resour. Res. 43, 1–10.
1007 doi:10.1029/2006WR005692

1008 NOAA's Ocean Service, Coastal Services Center, 2010. 2010 C-CAP Land Cover, Territory of
1009 American Samoa, Tutuila.

1010 Perreault, J., 2010. Development of a Water Budget in a Tropical Setting Accounting for
1011 Mountain Front Recharge: Tutuila, American Samoa. University of Hawai'i.

1012 Perroy, R.L., Bookhagen, B., Chadwick, O. a., Howarth, J.T., 2012. Holocene and Anthropocene
1013 Landscape Change: Arroyo Formation on Santa Cruz Island, California. Ann. Assoc. Am.
1014 Geogr. 102, 1229–1250. doi:10.1080/00045608.2012.715054

1015 Ramos-Scharrón, C.E., Macdonald, L.H., 2005. Measurement and prediction of sediment
1016 production from unpaved roads, St John, US Virgin Islands. Earth Surf. Process. Landforms
1017 30, 1283–1304.

1018 Ramos-Scharrón, C.E., Macdonald, L.H., 2007. Measurement and prediction of natural and
1019 anthropogenic sediment sources, St. John, US Virgin Islands. Catena 71, 250–266.

1020 Rankl, J.G., 2004. Relations Between Total-Sediment Load and Peak Discharge for Rainstorm
1021 Runoff on Five Ephemeral Streams in Wyoming. U.S. Geological Survey Water-Resources
1022 Investigations Report 02-4150. Denver, CO.

1023 Rapp, A., 1960. Recent development of mountain slopes in Karkevagge and surroundings,
1024 northern Scandinavia. Geogr. Ann. 42, 65–200.

1025 Reid, L.M., Dunne, T., 1984. Sediment production from forest road surfaces. Water Resour. Res.
1026 20, 1753–1761.

1027 Reid, L.M., Dunne, T., 1996. Rapid evaluation of sediment budgets. Catena Verlag, Reiskirchen,
1028 Germany.

1029 Risk, M.J., 2014. Assessing the effects of sediments and nutrients on coral reefs. Curr. Opin.
1030 Environ. Sustain. 7, 108–117. doi:10.1016/j.cosust.2014.01.003

1031 Rodrigues, J.O., Andrade, E.M., Ribeiro, L.A., 2013. Sediment loss in semiarid small watershed
1032 due to the land use. Rev. Ciência Agronômica 44, 488–498.

1033 Sadeghi, S.H.R., Mizuyama, T., Miyata, S., Gomi, T., Kosugi, K., Mizugaki, S., Onda, Y., 2007.
1034 Is MUSLE apt to small steeply reforested watershed? J. For. Res. 12, 270–277.
1035 doi:10.1007/s10310-007-0017-9

1036 Slaymaker, O., 2003. The sediment budget as conceptual framework and management tool.
1037 Hydrobiologia 494, 71–82.

1038 Stock, J.D., Rosener, M., Schmidt, K.M., Hanshaw, M.N., Brooks, B.A., Tribble, G., Jacobi, J.,
1039 2010. Sediment budget for a polluted Hawaiian reef using hillslope monitoring and process
1040 mapping, in: American Geophysical Union Fall Meeting. p. #EP22A–01.

1041 Stock, J.D., Tribble, G., 2010. Erosion and sediment loads from two Hawaiian watersheds, in:
1042 2nd Joint Federal Interagency Conference. Las Vegas, NV.

1043 Storlazzi, C.D., Norris, B.K., Rosenberger, K.J., 2015. The influence of grain size, grain color,
1044 and suspended-sediment concentration on light attenuation: Why fine-grained terrestrial
1045 sediment is bad for coral reef ecosystems. Coral Reefs 34, 967–975. doi:10.1007/s00338-
1046 015-1268-0

1047 Syvitski, J.P.M., Vörösmarty, C.J., Kettner, A.J., Green, P., 2005. Impact of humans on the flux
1048 of terrestrial sediment to the global coastal ocean. Science (80-.). 308, 376–380.
1049 doi:10.1126/science.1109454

1050 Thomas, S., Ridd, P. V, Day, G., 2003. Turbidity regimes over fringing coral reefs near a mining
1051 site at Lihir Island, Papua New Guinea. Mar. Pollut. Bull. 46, 1006–14. doi:10.1016/S0025-
1052 326X(03)00122-X

1053 Tonkin & Taylor International Ltd., 1989. Hydropower feasibility studies interim report - Phase
1054 1. Ref: 97/10163.

1055 Topping, J., 1972. Errors of Observation and their Treatment, 4th ed. Chapman and Hall,
1056 London, UK.

1057 Tropeano, D., 1991. High flow events, sediment transport in a small streams in the "Tertiary
1058 Basin" area in Piedmont (northwest Italy). Earth Surf. Process. Landforms 16, 323–339.

1059 Turnipseed, D.P., Sauer, V.B., 2010. Discharge Measurements at Gaging Stations, in: U.S.
1060 Geological Survey Techniques and Methods Book 3, Chap. A8. Reston, Va., p. 87.

1061 URS Company, 1978. American Samoa Water Resources Study: Assessment of Water Systems
1062 American Samoa. Coastal Zone Information Center, Honolulu, HI.

1063 Walling, D.E., 1977. Assessing the accuracy of suspended sediment rating curves for a small
1064 basin. Water Resour. Res. 13, 531–538.

1065 Walling, D.E., 1999. Linking land use, erosion and sediment yields in river basins.
1066 Hydrobiologia 410, 223–240.

1067 Walling, D.E., Collins, a. L., 2008. The catchment sediment budget as a management tool.
1068 Environ. Sci. Policy 11, 136–143. doi:10.1016/j.envsci.2007.10.004

1069 Wemple, B.C., Jones, J.A., Grant, G.E., 1996. Channel Network Extension by Logging Roads in
1070 Two Basins, Western Cascades, Oregon. Water Resour. Bull. 32, 1195–1207.

1071 West, K., van Woesik, R., 2001. Spatial and temporal variance of river discharge on Okinawa
1072 (Japan): inferring the temporal impact on adjacent coral reefs. Mar. Pollut. Bull. 42, 864–
1073 72.

1074 Wolman, M.G., Schick, A.P., 1967. Effects of construction on fluvial sediment, urban and
1075 suburban areas of Maryland. Water Resour. Res. 3, 451–464.

1076 Wong, M., 1996. Analysis of Streamflow Characteristics for Streams on the Island of Tutuila,
1077 American Samoa. U.S. Geological Survey Water-Resources Investigations Report 95-4185.

1078 Wulf, H., Bookhagen, B., Scherler, D., 2012. Climatic and geologic controls on suspended
1079 sediment flux in the Sutlej River Valley, western Himalaya. Hydrol. Earth Syst. Sci. 16,
1080 2193–2217. doi:10.5194/hess-16-2193-2012

1081 Zimmermann, A., Francke, T., Elsenbeer, H., 2012. Forests and erosion: Insights from a study of
1082 suspended-sediment dynamics in an overland flow-prone rainforest catchment. J. Hydrol.
1083 170–181.

1084

APPENDIX 1. Dams in Faga'alu watershed

Faga'alu stream was dammed at 4 locations above the village: 1) Matafao Dam (elevation 244 m) near the base of Mt. Matafao, draining 0.20 km², 2) Vaitanoa Dam at Virgin Falls (elevation 140 m), draining an additional 0.44 km², 3) a small unnamed dam below Vaitanoa Dam at elevation 100m, and 4) Lower Faga'alu Dam (elevation 48 m), immediately upstream of a large waterfall 30 m upstream of the quarry, draining an additional 0.26 km² (Tonkin & Taylor International Ltd., 1989). A 2012 aerial LiDAR survey (Photo Science, Inc.) indicates the drainage area at the Lower Faga'alu Dam is 0.90 km². A small stream capture/reservoir (~35 m³) is also present on a side tributary that joins Faga'alu stream on the south bank, opposite the quarry. It is connected to a ~6 cm diameter pipe but it is unknown when or by whom it was built, its initial capacity, or if it is still conveying water. During all site visits water was overtopping this small structure through the spillway crest, suggesting it is fed by a perennial stream.

Matafao Dam was constructed in 1917 for water supply to the Pago Pago Navy base, impounding a reservoir with initial capacity of 1.7 million gallons (6,400 m³) and piping the flow out of the watershed to a hydropower and water filtration plant in Fagatogo. In the early 1940's the Navy replaced the original cement tube pipeline and hydropower house with cast iron pipe but it is unknown when the scheme fell out of use (Tonkin & Taylor International Ltd., 1989; URS Company, 1978). Remote sensing and a site visit on 6/21/13 confirmed the reservoir is still filling to the spillway crest with water and routing some flow to the Fagatogo site, though the amount is much less than the 10 in. diameter pipes conveyance capacity and the flow rate variability is unknown. A previous site visit on 2/21/13 by American Samoa Power Authority (ASPA) found the reservoir empty of water but filled with an estimated 3-5 meters of fine sediment (Kearns, 2013). Interviews with local maintenance staff and historical photos

confirmed the Matafao Reservoir was actively maintained and cleaned of sediment until the early 70's.

The Vaitanoa (Virgin Falls) Dam, was built in 1964 to provide drinking water but the pipe was not completed as of 10/19/89, and a stockpile of some 40 (8 ft. length) 8 in. diameter asbestos-cement pipes was found on the streambanks. Local quarry staff recall the pipes were removed from the site sometime in the 1990's. The Vaitanoa Reservoir had a design volume of 4.5 million gallons (17,000m^3), but is assumed to be full of sediment since the drainage valves were never opened and the reservoir was overtopping the spillway as of 10/18/89 (Tonkin & Taylor International Ltd., 1989). A low masonry weir was also constructed downstream of the Vaitanoa Dam, but not connected to any piping.

The Lower Faga'alu Dam was constructed in 1966/67 just above the Samoa Maritime, Ltd. Quarry, as a source of water for the LBJ Medical Centre. It is unknown when this dam went out of use but in 1989 the 8 in. conveyance pipe was badly leaking and presumed out of service. The 8 in. pipe disappears below the floor of the Samoa Maritime quarry and it is unknown if it is still conveying water or has plugged with sediment. The derelict filtration plant at the entrance to the quarry was disconnected prior to 1989 (Tonkin & Taylor International Ltd., 1989). The original capacity was 0.03 million gallons (114 m^3) but is now full of coarse sediment up to the spillway crest. No reports were found indicating this structure was ever emptied of sediment.

APPENDIX 2. Stream gaging in Faga'alu Watershed

Stream gaging sites were chosen to take advantage of an existing control structure at FG1 (Figure A2.1) and a stabilized stream cross section at FG3 (Figure A2.2)(Duvert and Gratiot, 2010). At FG1 and FG3, Q was calculated from 15 minute interval stream stage measurements, using a stage-Q rating curve calibrated to manual Q measurements made under baseflow and

stormflow conditions (Figures A2.3 and A2.4). Stream stage was measured with non-vented pressure transducers (PT) (Solinst Levelogger or Onset HOBO Water Level Logger) installed in stilling wells at FG1 and FG3. Barometric pressure data collected at Wx were used to calculate stage from the pressure data recorded by the PT. Data gaps in barometric pressure from Wx were filled by data from stations at Pago Pago Harbor (NSTP6) and NOAA Climate Observatory at Tula (TULA) (Figure 1). Priority was given to the station closest to the watershed with valid barometric pressure data. Barometric data were highly correlated and the data source made little (<1cm) difference in the resulting water level. Q was measured in the field by the area-velocity method (AV) using a Marsh-McBirney flowmeter to measure flow velocity and channel surveys measure cross-sectional area (Harrelson et al., 1994; Turnipseed and Sauer, 2010).

AV-Q measurements could not be made at high stages at FG1 and FG3 for safety reasons, so stage-Q relationships were constructed to estimate a continuous record of Q. At FG3, the channel is rectangular with stabilized rip-rap on the banks and bed (Figure A2.2). Recorded stage varied from 4 to 147 cm. AV-Q measurements (n= 14) were made from 30 to 1,558.0 L/sec, covering a range of stages from 6 to 39 cm. The highest recorded stage was much higher than the highest stage with measured Q so the rating could not be extrapolated by a power law. Stream conditions at FG3 fit the assumption for Manning's equation, so the stage-Q rating at FG3 was created using Manning's equation, calibrating Manning's n (0.067) to the Q measurements (Figure A2.3).

At FG1, the flow control structure is a masonry ogee spillway crest of a defunct stream capture. The structure is a rectangular channel 43 cm deep that transitions abruptly to gently sloping banks, causing an abrupt change in the stage-Q relationship (Figure A2.1). At FG1, recorded stage height ranged from 4 to 120 cm, while area-velocity Q measurements (n= 22)

covered stages from 6 to 17 cm. Since the highest recorded stage (120 cm) was higher than the highest stage with measured Q (17 cm), and there was a distinct change in channel geometry above 43 cm the rating could not be extrapolated by a power law. The flow structure did not meet the assumptions for using Manning's equation to predict flow so the HEC-RAS model was used (Brunner, 2010). The surveyed geometry of the upstream channel and flow structure at FG1 were input to HEC-RAS, and the HEC-RAS model was calibrated to the Q measurements (Figure A2.4). While a power function fit Q measurements better than HEC-RAS for low flow, HEC-RAS fit better for Q above the storm threshold used in analyses of SSY (Figure A2.4).

APPENDIX 3. Water discharge during storm events

Insert Table A3.1 here

APPENDIX 4. Turbidity-Suspended Sediment Concentration rating curves for turbidimeters in Faga'alu

Turbidity (T) was measured at FG1 and FG3 using three types of turbidimeters: 1) Greenspan TS3000 (TS), 2) YSI 600OMS with 6136 turbidity probe (YSI), and 3) Campbell Scientific OBS500 (OBS). All turbidimeters were permanently installed in protective PVC housings near the streambed where the turbidity probe would be submerged at all flow conditions, with the turbidity probe oriented downstream. Despite regular maintenance, debris fouling during storm and baseflows was common and caused data loss during several storm events. Storm events with incomplete or invalid T data were not used in the analysis. A three-point calibration was performed on the YSI turbidimeter with YSI turbidity standards (0, 126, and 1000 NTU) at the beginning of each field season and approximately every 3-6 months during data collection. Turbidity measured with 0, 126, and 1000 NTU standards differed by less

than 10% (4-8%) during each recalibration. The OBS requires calibration every two years, so recalibration was not needed during the study period. All turbidimeters were cleaned following storms to ensure proper operation.

At FG3, a YSI turbidimeter recorded T (NTU) at 5 min intervals from January 30, 2012, to February 20, 2012, and at 15 min intervals from February 27, 2012 to May 23, 2012, when it was damaged during a large storm. The YSI turbidimeter was replaced with an OBS, which recorded Backscatter (BS) and Sidescatter (SS) at 5 min intervals from March 7, 2013, to July 15, 2014 (OBSa), and was resampled to 15 min intervals. No data was recorded from August 2013-January 2014 when the wiper clogged with sediment. A new OBS was installed at FG3 from January, 2014, to August, 2014 (OBSb). To correct for some periods of high noise observed in the BS and SS data recorded by the OBSa in 2013, the OBSb installed in 2014 was programmed to make a burst of 100 BS and SS measurements at 15 min intervals, and record Median, Mean, STD, Min, and Max. All BS and SS parameters were analyzed to determine which showed the best relationship with SSC. Mean SS showed the highest r^2 and is a physically comparable measurement to NTU measured by the YSI and TS (Anderson, 2005).

At FG1, the TS turbidimeter recorded T (NTU) at 5 min intervals from January 2012 until it was vandalized and destroyed in July 2012. The YSI turbidimeter, previously deployed at FG3 in 2012, was repaired and redeployed at FG1 and recorded T (NTU) at 5 min intervals from June 2013 to October 2013, and January 2014 to August 2014. T data was resampled to 15 min intervals to compare with SSC samples for the T-SSC relationship, and to correspond to Q for calculating SSY.

The T-SSC relationship can be unique to each region, stream, instrument or even each storm event (Lewis et al., 2001), and can be influenced by water color, dissolved solids and

organic matter, temperature, and the shape, size, and composition of sediment. However, T has proved to be a robust surrogate measure of SSC in streams (Gippel, 1995), and is most accurate when a unique T-SSC relationship is developed for each instrument separately, using in situ grab samples under storm conditions (Lewis, 1996). A unique T-SSC relationship was developed for each turbidimeter, at each location, using 15 min interval T data and SSC samples from storm periods only (Figure A4.1). A "synthetic" T-SSC relationship was also developed by placing the turbidimeter in a black tub with water, and sampling T and SSC as sediment was added (Figure 4.2), but results were not comparable to T-SSC relationships developed under actual storm conditions and were not used in further analyses.

The T-SSC relationships varied among sampling sites and sensors but all showed acceptable r^2 values (0.79-0.99). Lower scatter was achieved by using grab samples collected during stormflows only. For the TS (not shown) and YSI deployed at FG1, the r2 values were high (0.58, 0.99) but the ranges of T and SSC values used to develop the relationships were considered too small (0-16 NTU) compared to the maximum observed during the deployment period (1,077 NTU) to develop a robust relationship for higher T values. Instead, the T-SSC relationship developed for the YSI turbidimeter installed at FG3 (Figure A4.1a) was used to calculate SSC from T data collected by the TS and the YSI at FG1. For the YSI turbidimeter, more scatter was observed in the T-SSC relationship at FG3 than at FG1 (Figure A4.1a), which could be attributed to the higher number and wider range of values sampled, and to temporal variability in sediment characteristics. The OBSa and OBSb turbidimeters had high r2 values (0.82, 0.93) and compared well between the two periods of deployment (Figure A4.1b).

Figure Captions

Figure 1. Faga'alu watershed showing the UPPER (undisturbed) and LOWER (human-disturbed) subwatersheds. The LOWER subwatershed drains areas between FG1 and FG3, and is further subdivided into the LOWER_QUARRY containing the quarry (between FG1 and FG2) and the LOWER_VILLAGE containing the village areas (between FG2 and FG3). The TOTAL watershed includes all subwatersheds draining to FG3. The Administrative watershed boundary for government jurisdiction is outlined by the dotted grey line. Blue pentagons in the UPPER watershed show the location of abandoned water supply reservoirs (see Appendix 1 for full description). Barometer locations at NSTP6 and TULA are shown in top-right.

Figure 2. Photos of the aggregate quarry in Faga'alu in 2012, 2013, and 2014. Pictures a-b show vegetation overgrowth during the period of study from 2012-2014, and the location of the groundwater diversion that was installed in 2012. Pictures c-d show that haul roads were covered in gravel in 2013. Photos: Messina

Figure 3. Time series of water discharge (Q), calculated from measured stage and the stage-discharge rating curves in a) 2012 b) 2013 and c) 2014.

Figure 4. Example of a storm event (02/14/2014). SSY at FG1 and FG3 calculated from SSC modeled from T, and SSY at FG2 from SSC samples collected by the Autosampler.

Figure 5. Boxplots of Suspended Sediment Concentration (SSC) from grab samples only (no Autosampler) at FG1, FG2, and FG3 during (a) non-stormflow and (b) stormflow.

Figure 6. Water Discharge versus suspended sediment concentration measured from grab samples at a) FG1, b) FG2, and c) FG3 during non-stormflow and stormflow periods. The box in b) highlights the samples with high SSC during low flows. Solid symbols indicate SSC samples where precipitation during the preceding 24 hours was 0 mm.

Figure 7. $sSSY_{EV}$ regression models for predictive storm metrics. Each point represents a different storm event. **=slopes and intercepts were statistically different ($p<0.01$), *=intercepts were statistically different ($p<0.01$).

Figure A2.1. Stream cross-section at FG1

Figure A2.2. Stream cross-section at FG3

Figure A2.3. Stage-Discharge relationships for stream gaging site at FG3 for (a) the full range of observed stage and (b) the range of stages with AV measurements of Q. RMSE was 93 L/sec, or 32% of observed Q.

Figure A2.4. Stage-Discharge relationships for stream gaging site at FG1 for (a) the full range of observed stage and (b) the range of stages with AV measurements of Q. RMSE was 31 L/sec, or 22% of observed Q. "Channel Top" refers to the point where the rectangular channel transitions to a sloped bank and cross-sectional area increases much more rapidly with stage. A power-law

relationship is also displayed to illustrate the potential error that could result if inappropriate methods are used.

Figure A3.1. Example of method for separating storms based on baseflow separation. Black line is hydrograph, grey line is baseflow calculated by R statistical package EcoHydRology. Storm periods are shaded in grey. Seven storm events are identified from March 3, 2013 to March 13, 2013.

Figure A4.1. Turbidity-Suspended Sediment Concentration relationships for a) the YSI turbidimeter deployed at FG3 (02/27/2012-05/23/2012) and the same YSI turbidimeter deployed at FG1 (06/13/2013-12/31/2014). b) OBS500 turbidimeter deployed at FG3 (03/11/2013-07/11/2013) and c) OBS500 turbidimeter deployed at FG3 (01/31/2014-03/04/2014).

Figure A4.2. Synthetic Rating Curves for (a) OBS turbidimeter deployed at FG3 and (b) YSI deployed at FG1.

Figure

Click here to download high resolution image

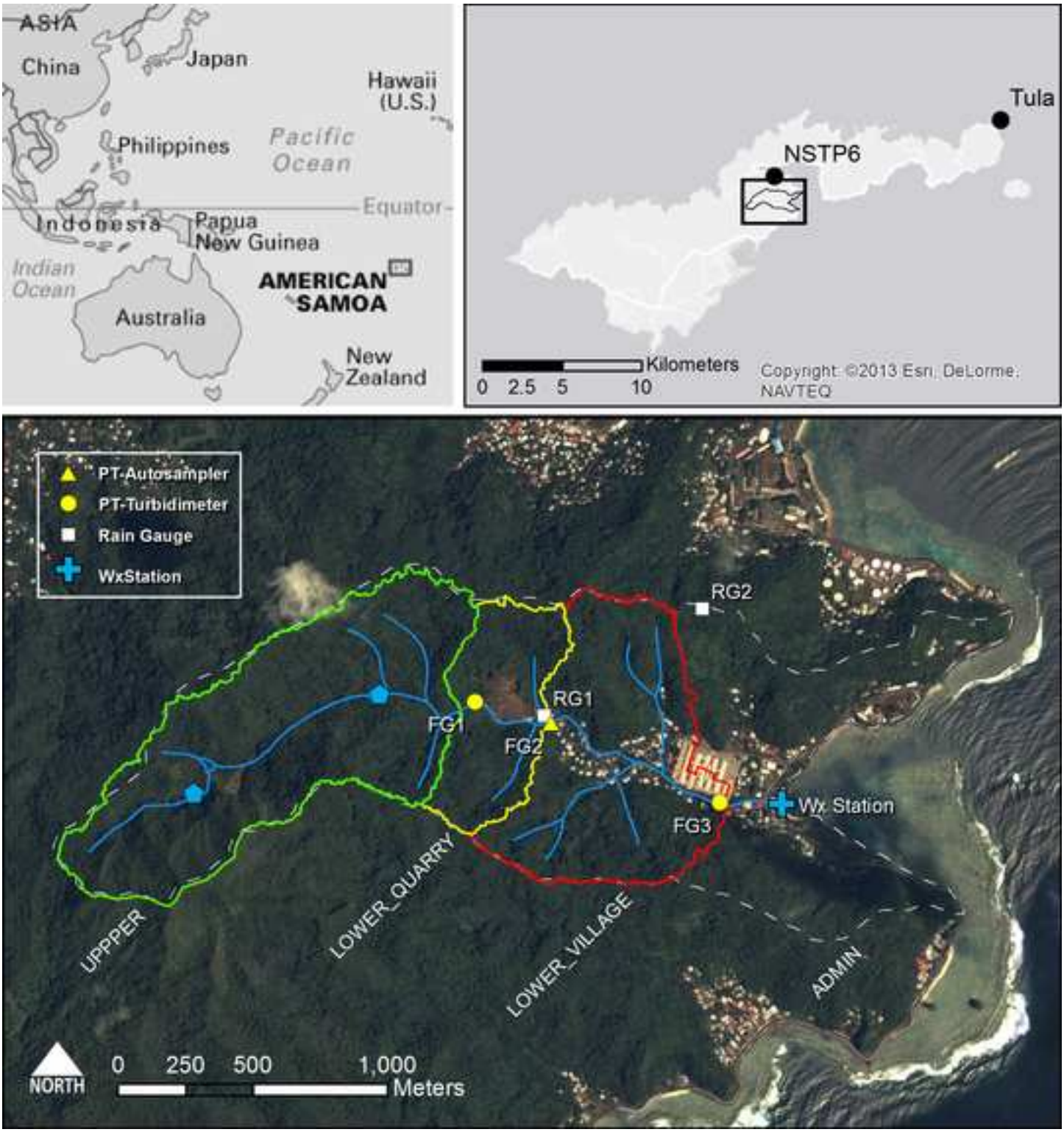

Figure
Click here to download high resolution image

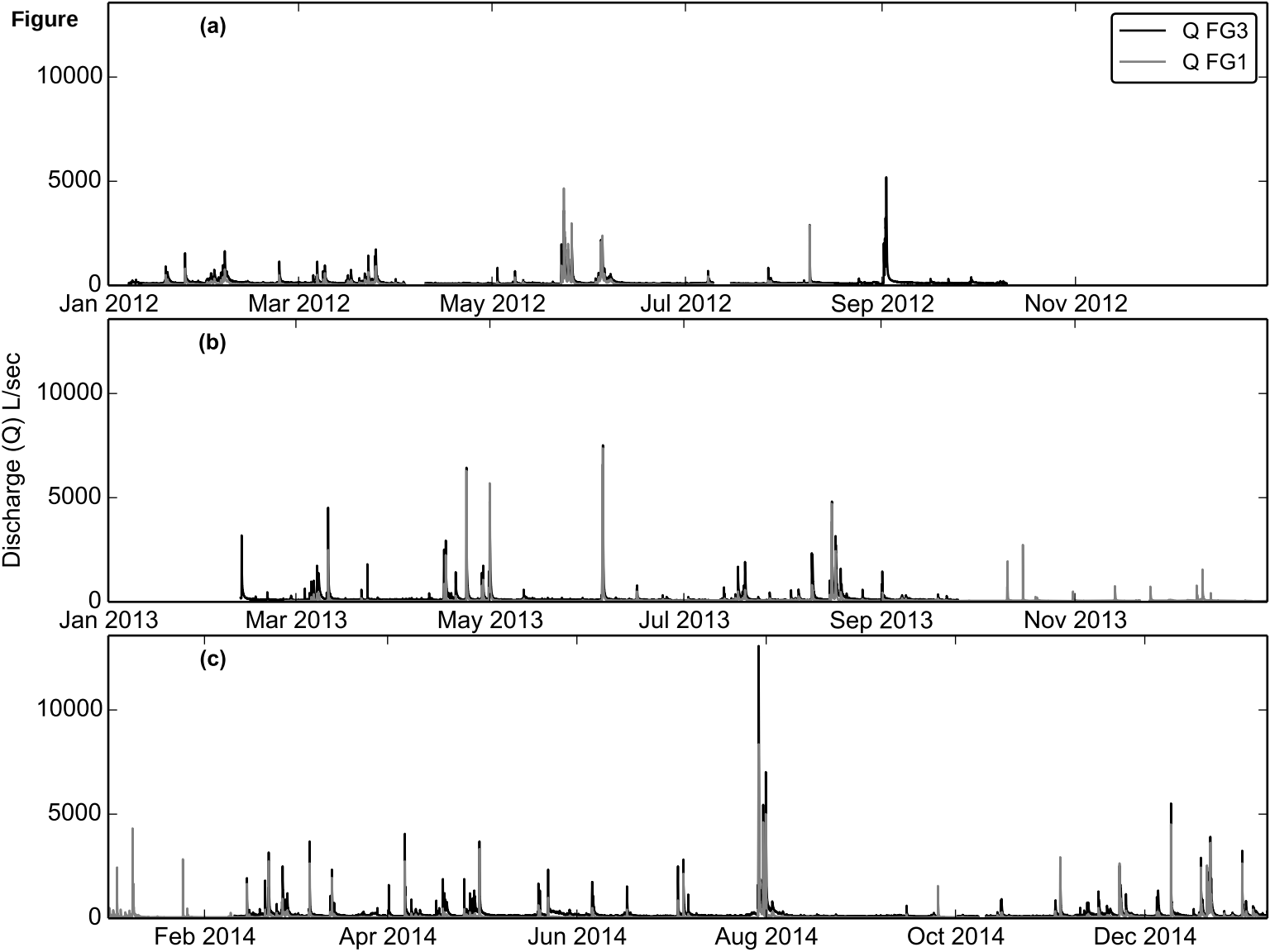
Figure
(a)
(b)
(c)
Q FG3
Q FG1
Discharge (Q) L/sec
10000
5000
0
Jan 2012
Mar 2012
May 2012
Jul 2012
Sep 2012
Nov 2012
Jan 2013
Mar 2013
May 2013
Jul 2013
Sep 2013
Nov 2013
Feb 2014
Apr 2014
Jun 2014
Aug 2014
Oct 2014
Dec 2014

Figure

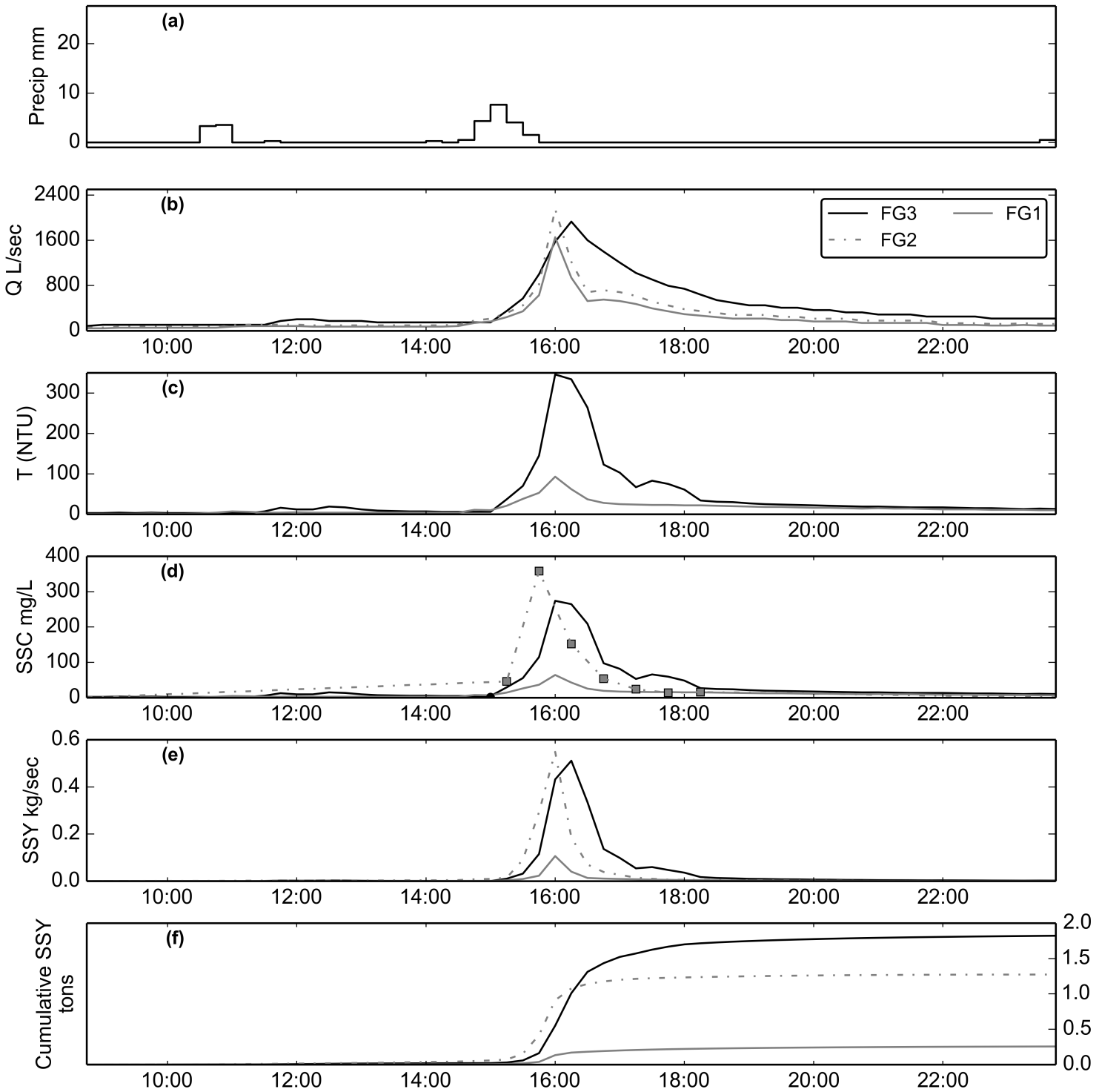
(a)
Precip mm
20
10
0
(b)
Q L/sec
2400
1600
800
0
FG3
FG1
FG2
10:00
12:00
14:00
16:00
18:00
20:00
22:00
(c)
T (NTU)
300
200
100
0
(d)
SSC mg/L
400
300
200
100
0
(e)
SSY kg/sec
0.6
0.4
0.2
0.0
(f)
Cumulative SSY
tons
2.0
1.5
1.0
0.5
0.0

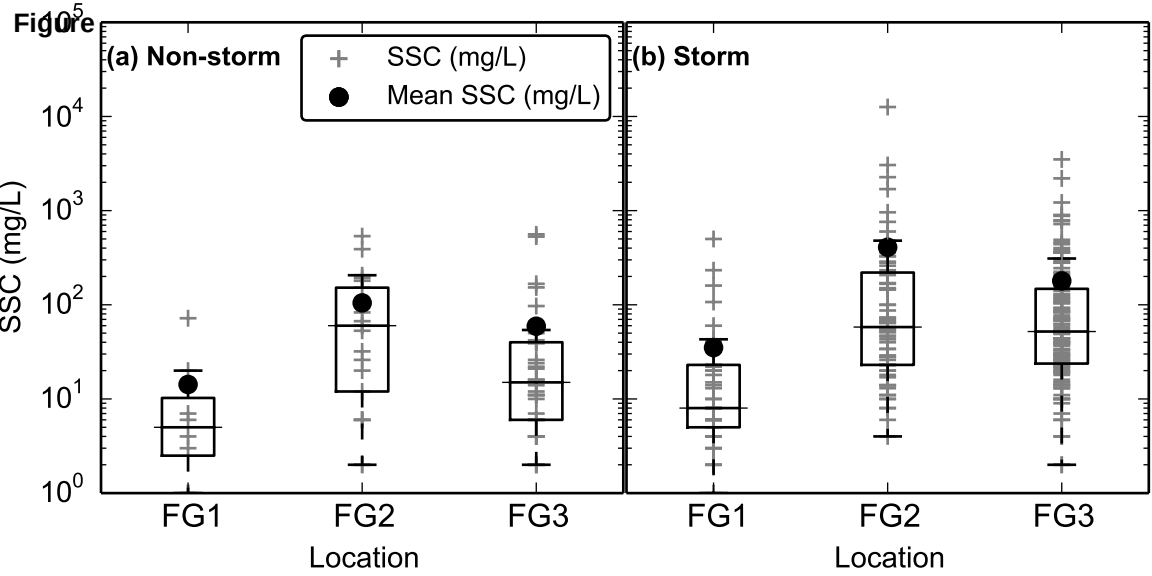
Figure
(a) Non-storm
(b) Storm
SSC (mg/L)
Mean SSC (mg/L)
SSC (mg/L)
10^5
10^4
10^3
10^2
10^1
10^0
FG1
FG2
FG3
Location

Figure

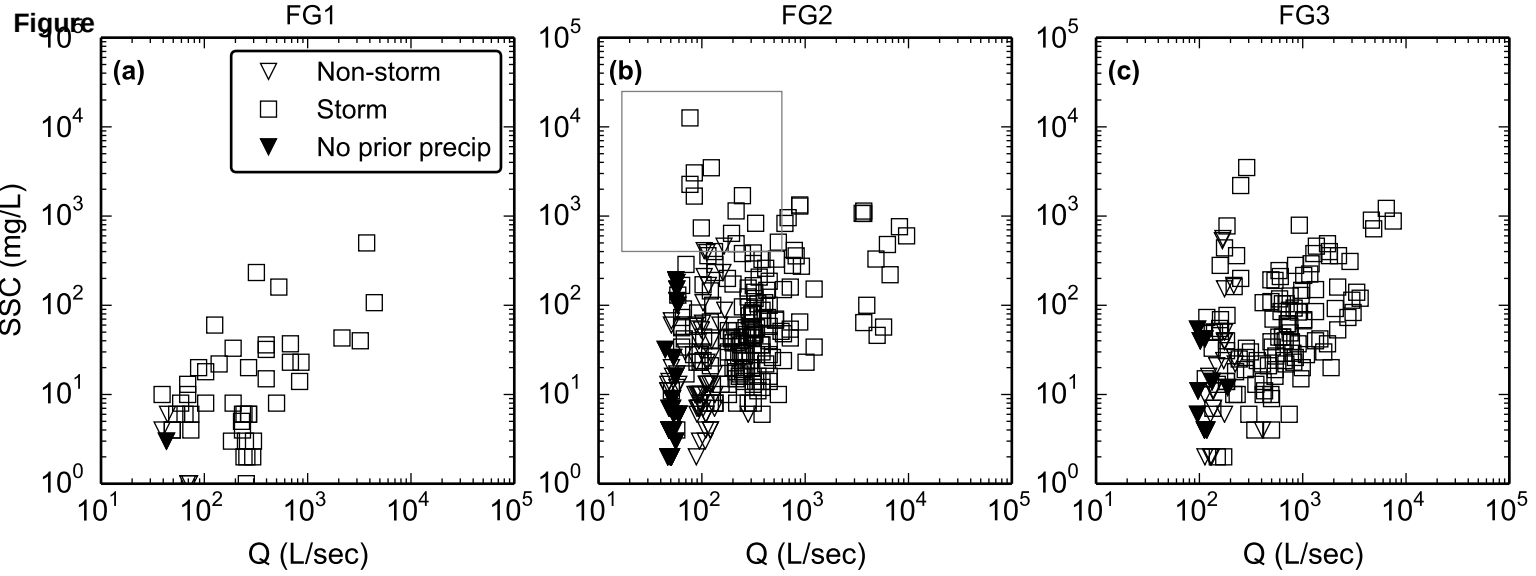
FG1
FG2
FG3
(a)
(b)
(c)
Non-storm
Storm
No prior precip
SSC (mg/L)
Q (L/sec)
Q (L/sec)
Q (L/sec)

Figure 8

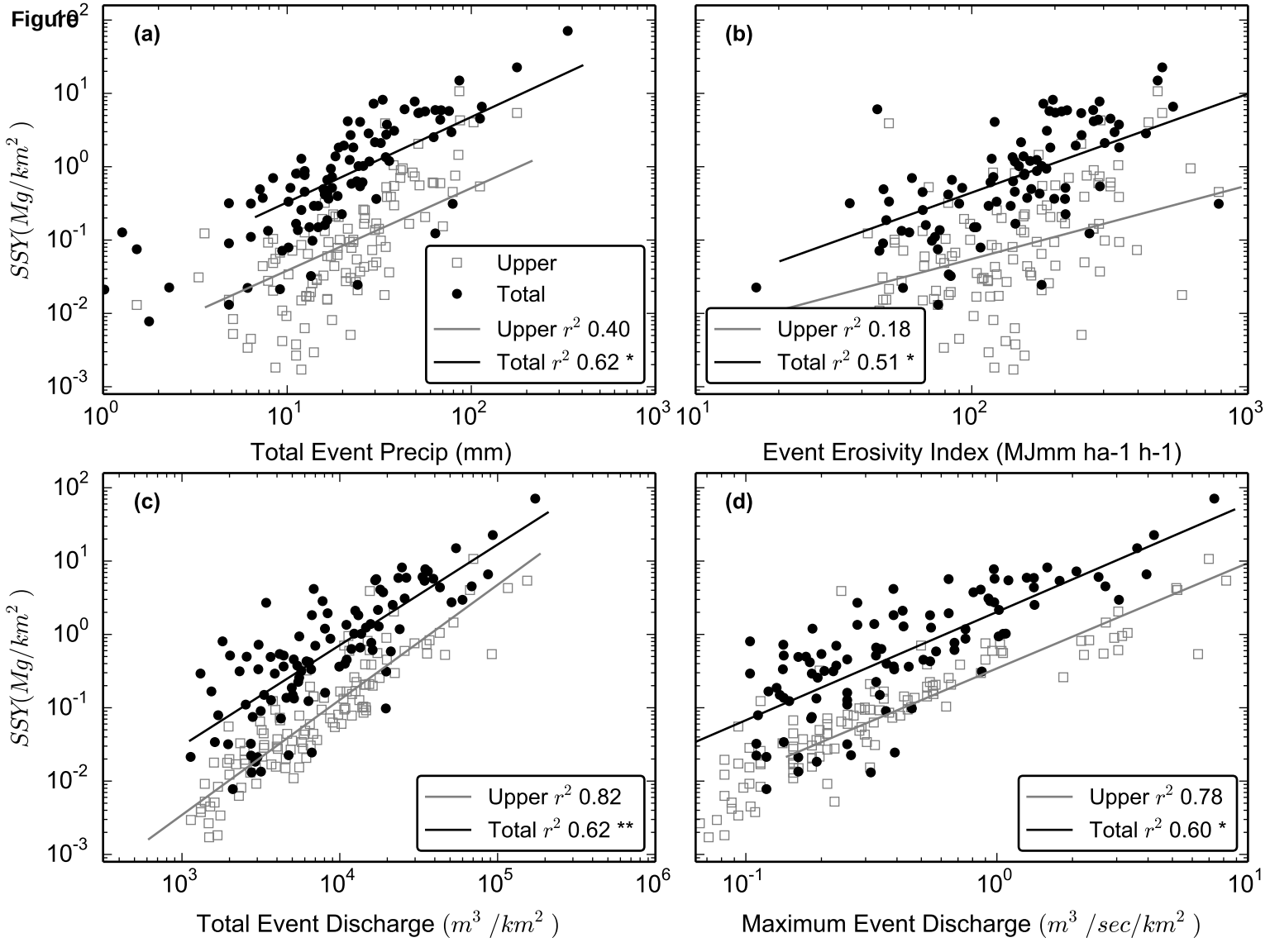
(a)
(b)
(c)
(d)
$SSY(Mg/km^2)$
Upper
Total
Upper r^2 0.40
Total r^2 0.62 *
Total Event Precip (mm)
Upper r^2 0.18
Total r^2 0.51 *
Event Erosivity Index (MJmm ha-1 h-1)
Upper r^2 0.82
Total r^2 0.62 **
Total Event Discharge (m^3/km^2)
Upper r^2 0.78
Total r^2 0.60 *
Maximum Event Discharge $(m^3/sec/km^2)$

Figure

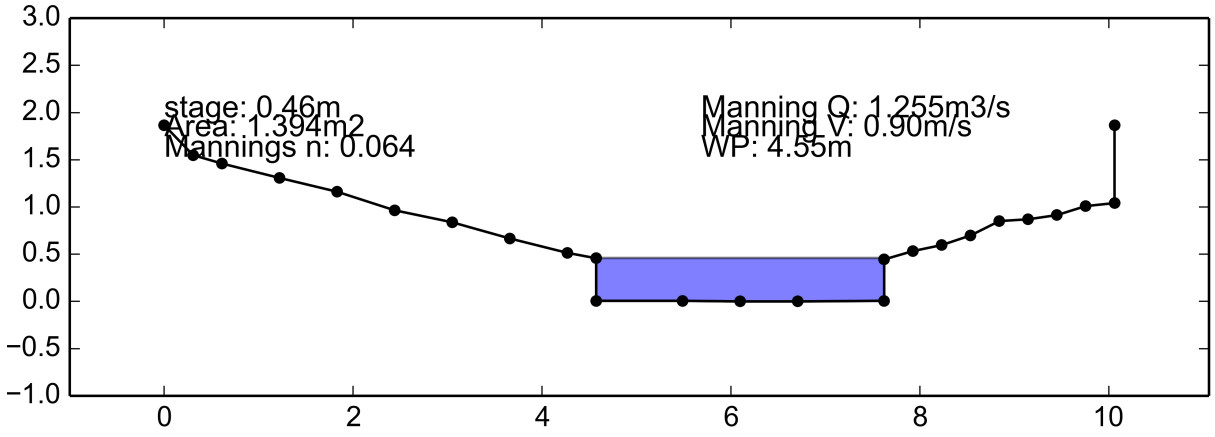
stage: 0.46m
Area: 1.394m2
Mannings n: 0.064
Manning Q: 1.255m3/s
Manning V: 0.90m/s
WP: 4.55m
3.0
2.5
2.0
1.5
1.0
0.5
0.0
−0.5
−1.0
0
2
4
6
8
10

Figure

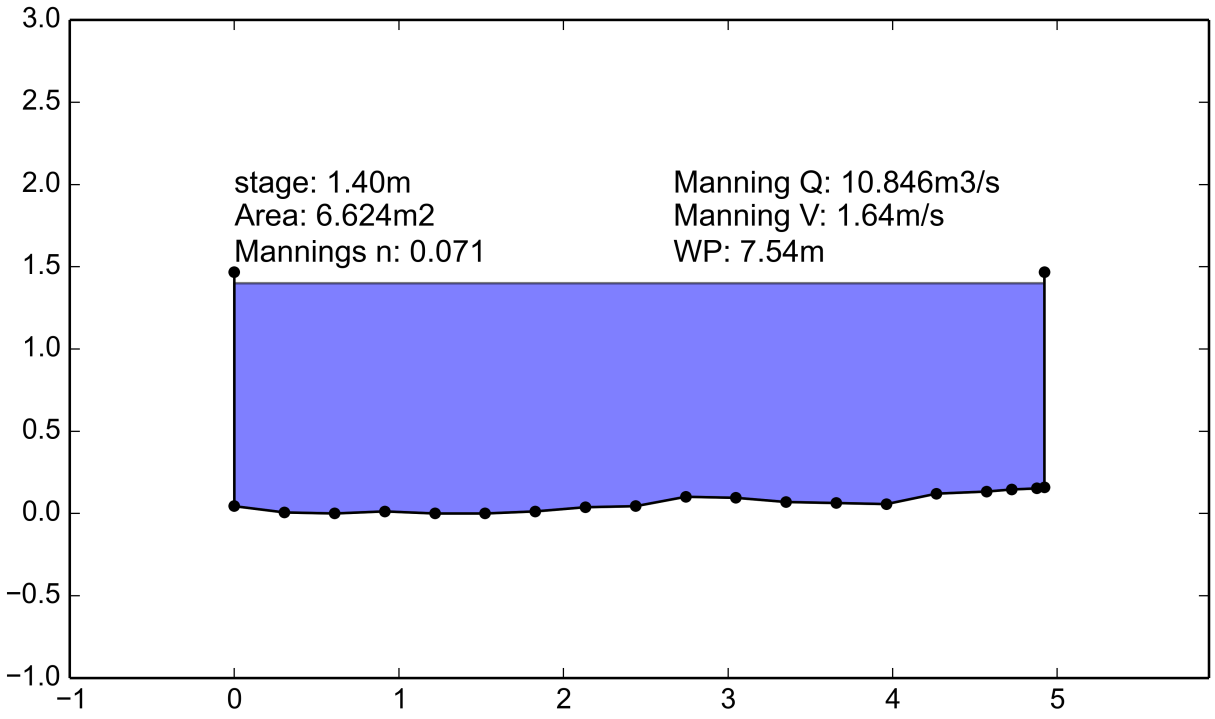
stage: 1.40m
Area: 6.624m2
Mannings n: 0.071
Manning Q: 10.846m3/s
Manning V: 1.64m/s
WP: 7.54m
3.0
2.5
2.0
1.5
1.0
0.5
0.0
−0.5
−1.0
−1
0
1
2
3
4
5

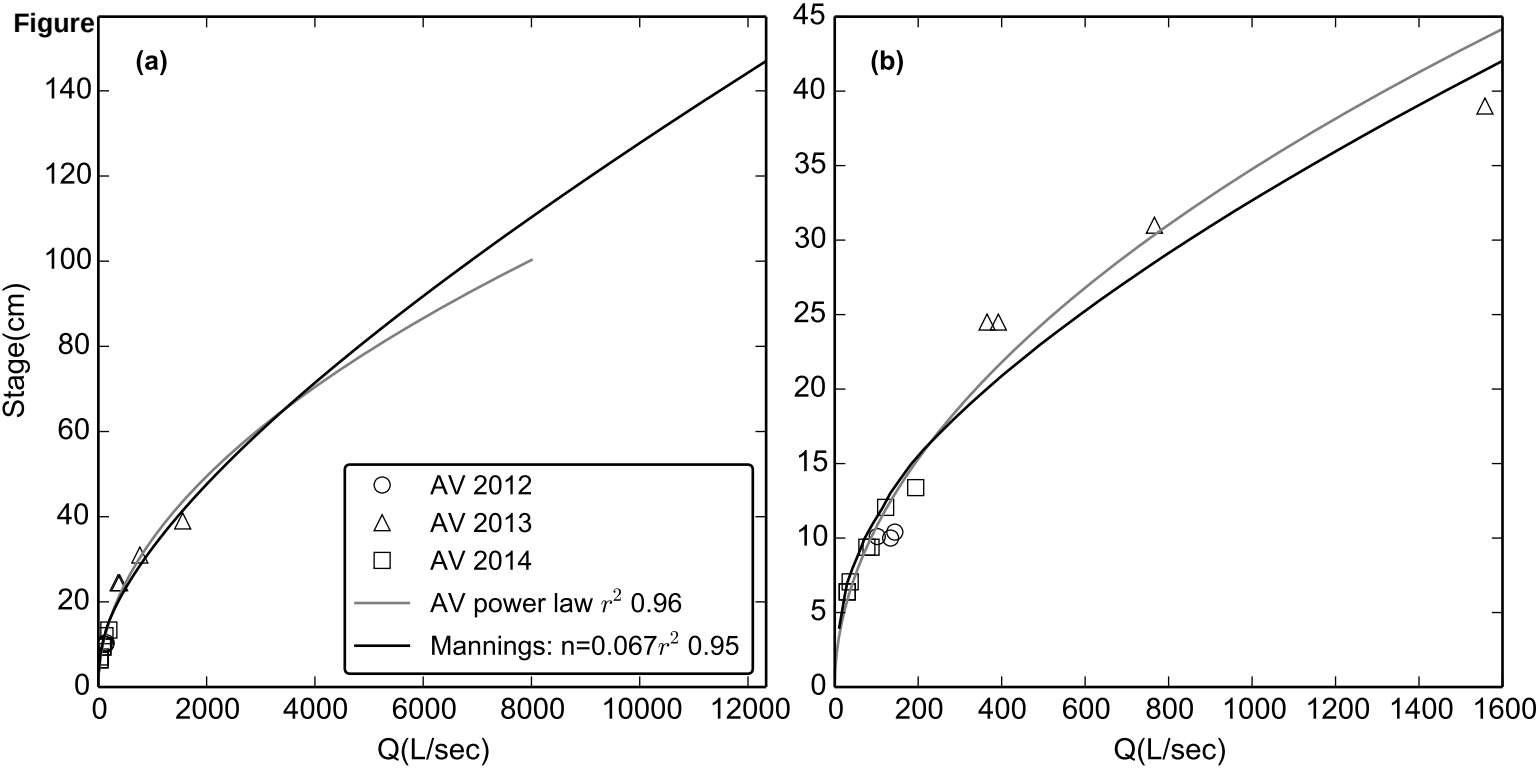
Figure
(a)
(b)
Stage(cm)
Q(L/sec)
Q(L/sec)
AV 2012
AV 2013
AV 2014
AV power law r^2 0.96
Mannings: n=0.067r^2 0.95

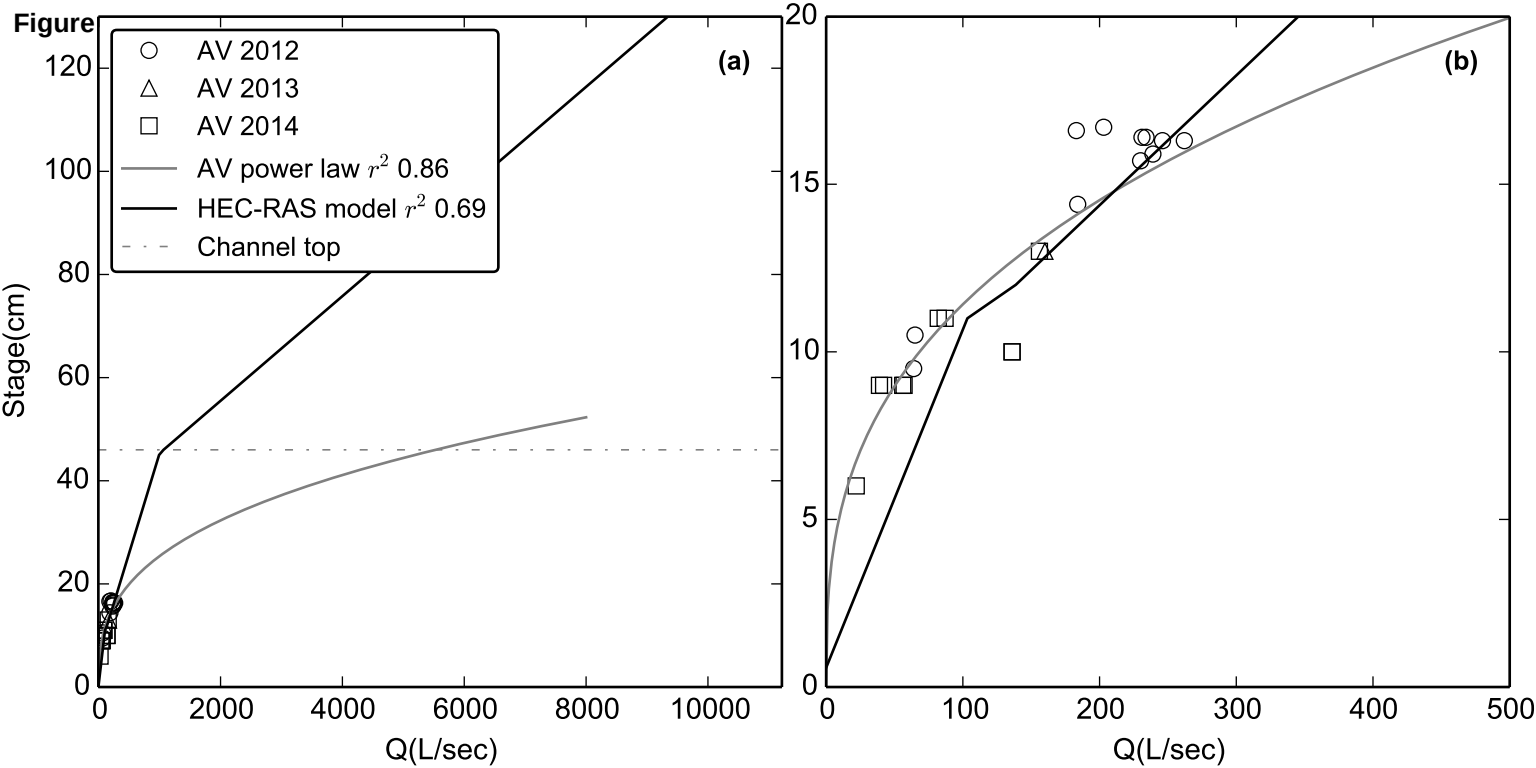
Figure
AV 2012
AV 2013
AV 2014
AV power law r^2 0.86
HEC-RAS model r^2 0.69
Channel top
(a)
(b)
Stage(cm)
Q(L/sec)
Q(L/sec)
0
20
40
60
80
100
120
0
2000
4000
6000
8000
10000
0
5
10
15
20
0
100
200
300
400
500

Figure

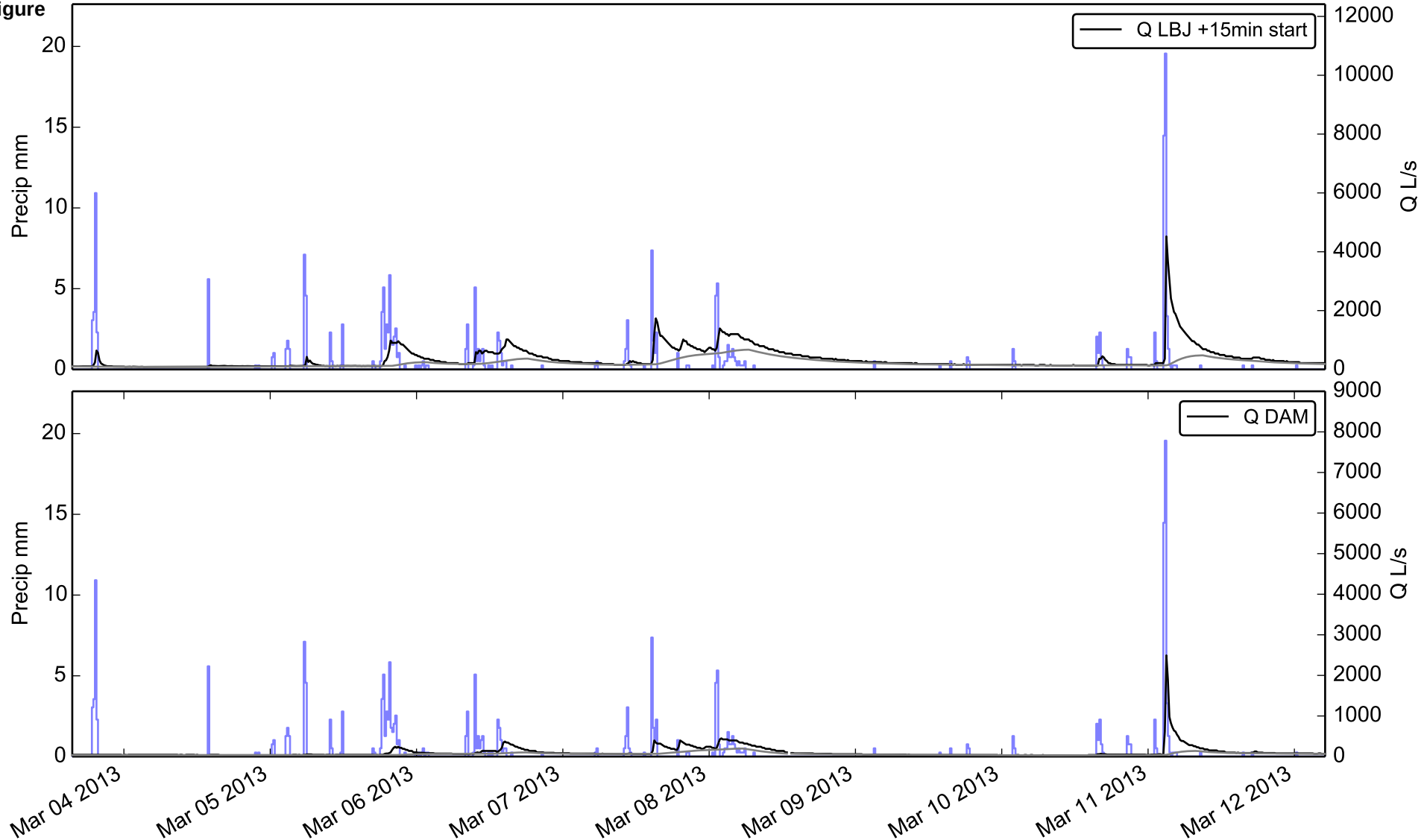
Q LBJ +15min start
Precip mm
Q L/s
Q DAM
Precip mm
Q L/s
Mar 04 2013
Mar 05 2013
Mar 06 2013
Mar 07 2013
Mar 08 2013
Mar 09 2013
Mar 10 2013
Mar 11 2013
Mar 12 2013

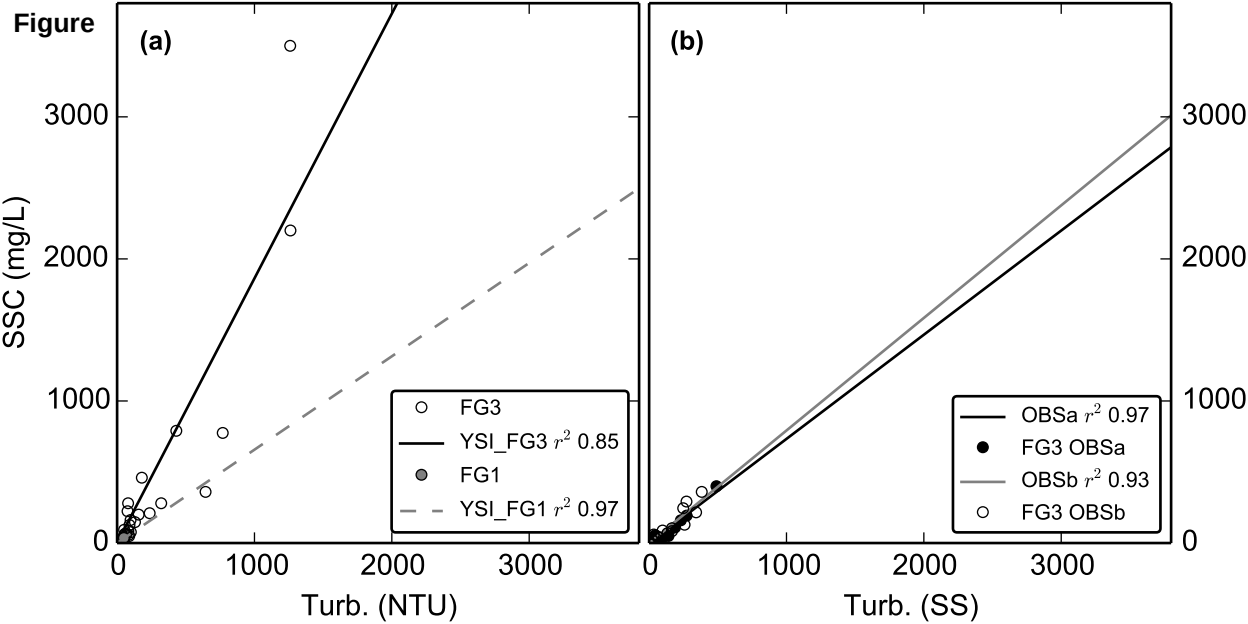
Figure
(a)
(b)
SSC (mg/L)
Turb. (NTU)
Turb. (SS)
0
1000
2000
3000
FG3
YSI_FG3 r^2 0.85
FG1
YSI_FG1 r^2 0.97
OBSa r^2 0.97
FG3 OBSa
OBSb r^2 0.93
FG3 OBSb

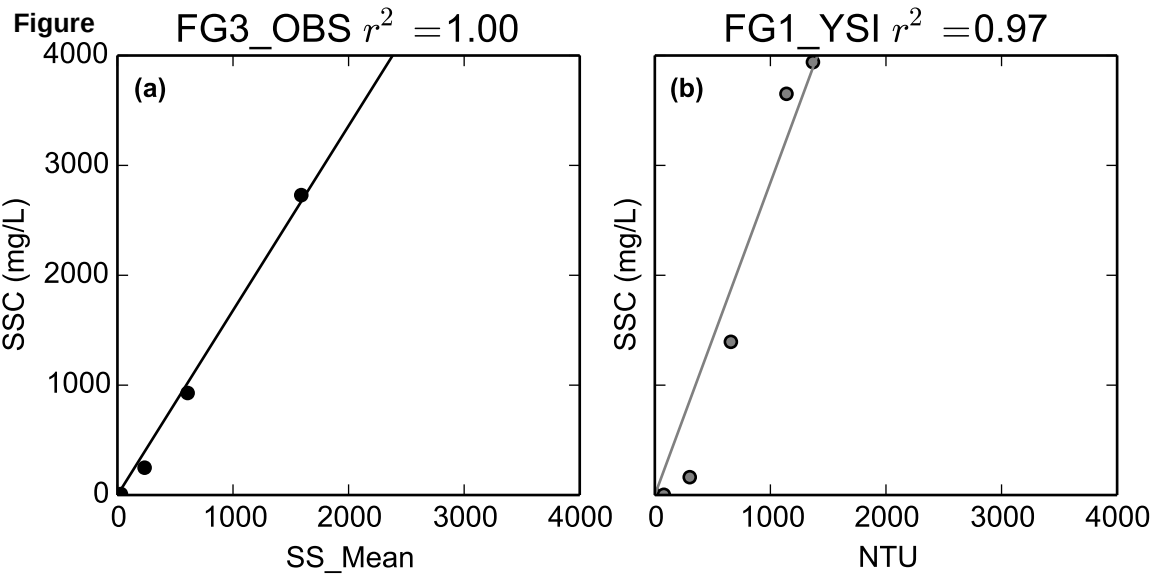
Figure
FG3_OBS r^2 =1.00
(a)
SSC (mg/L)
SS_Mean
0
1000
2000
3000
4000
FG1_YSI r^2 =0.97
(b)
SSC (mg/L)
NTU
0
1000
2000
3000
4000

Table

Click here to download Table: Table1_landcover.pdf

Table 1. Land use categories in Faga'alu subwatersheds (NOAA Ocean Service and Coastal Services Center, 2010). Land cover percentages are of the subwatershed.

Subwatershed (pourpoint)	Cumulative Area		Subwatershed Area		Land cover as % subwatershed area [a]							
	km^2	%	km^2	%	B	HI	DOS	GA	F	S	Disturbed	Undisturbed
UPPER (FG1)	0.9	50	0.90	50	0.4	0.0	0.0	0.1	82	17.1	0.4	100
LOWER_QUARRY (FG2)	1.2	66	0.27	16	5.7	0.7	0.1	0.5	92	0.9	6.5	94
LOWER_VILLAGE (FG3)	1.8	100	0.60	34	0.0	9.0	2.6	0.2	88	0.6	11.7	88
LOWER (FG3)	1.8	100	0.88	50	1.8	6.4	1.8	0.3	89	0.7	10.1	90
TOTAL (FG3)	1.8	100	1.78	100	1.1	3.2	0.9	0.2	86	9.0	5.2	95

a. B=Bare, HI=High Intensity Developed, DOS=Developed Open Space, GA=Grassland (agriculture), F=Forest, S=Scrub/Shrub, Disturbed=B+HI+DOS+GA, Undisturbed=F+S

Table

Click here to download Table: Table2_S_budget_pre.pdf

Table 2. Event-wise suspended sediment yield (SSY_{EV}) from subwatersheds in Faga'alu for events with simultaneous data from FG1 and FG3. Storm numbers correspond with the storms presented in Table A3.1.

	Storm	Precip	SSY_{EV} tons			% of SSY_{EV} TOTAL		PE[a]		SSC
Storm#	Start	mm	UPPER[b]	LOWER[c]	TOTAL[d]	UPPER	LOWER	UPPER	TOTAL	Data Source
2	01/19/2012	18	0.06	0.63	0.69	8.0	91.0	49	36	int. grab
4	01/31/2012	35	0.03	1.92	1.95	1.0	98.0	49	118	T-YSI
5	02/01/2012	11	0.01	0.4	0.42	3.0	96.0	49	118	T-YSI
6	02/02/2012	16	0.06	1.02	1.08	5.0	94.0	49	118	T-YSI
7	02/03/2012	11	0.08	2.01	2.09	3.0	96.0	49	118	T-YSI
8	02/04/2012	6	0.0	0.51	0.51	0.0	99.0	49	118	T-YSI
9	02/05/2012	23	0.05	0.98	1.03	5.0	94.0	49	118	T-YSI
10	02/05/2012	21	0.09	1.93	2.02	4.0	95.0	49	118	T-YSI
11	02/06/2012	38	0.28	4.75	5.03	5.0	94.0	49	118	T-YSI
12	02/07/2012	4	0.01	0.13	0.15	9.0	90.0	49	118	T-YSI
13	02/07/2012	10	0.03	0.51	0.54	5.0	94.0	49	118	T-YSI
14	02/13/2012	11	0.0	0.27	0.27	1.0	98.0	49	118	T-YSI
16	03/05/2012	22	0.0	4.39	4.4	0.0	99.0	49	118	T-YSI
17	03/06/2012	56	0.19	9.05	9.25	2.0	97.0	49	118	T-YSI
18	03/08/2012	22	0.09	2.89	2.98	2.0	97.0	49	118	T-YSI
19	03/09/2012	19	0.2	2.78	2.97	6.0	93.0	49	118	T-YSI
20	03/15/2012	17	0.01	1.17	1.18	0.0	99.0	49	118	T-YSI
21	03/16/2012	34	0.08	2.12	2.2	3.0	96.0	49	118	T-YSI
22	03/17/2012	32	0.09	3.33	3.43	2.0	97.0	49	118	T-YSI
23	03/20/2012	24	0.04	0.84	0.88	4.0	95.0	49	118	T-YSI
24	03/21/2012	18	0.2	2.06	2.26	8.0	91.0	49	118	T-YSI
25	03/22/2012	34	0.37	5.75	6.12	5.0	94.0	49	118	T-YSI
27	03/24/2012	7	0.03	0.19	0.22	12.0	87.0	49	118	T-YSI
28	03/25/2012	49	0.7	11.92	12.62	5.0	94.0	49	118	T-YSI
29	03/31/2012	15	0.03	0.78	0.81	3.0	96.0	49	118	T-YSI
32	05/07/2012	11	0.0	1.31	1.31	0.0	99.0	49	118	T-YSI
33	05/08/2012	21	0.13	6.65	6.79	1.0	98.0	49	118	T-YSI
34	05/20/2012	13	0.0	0.47	0.48	0.0	99.0	49	118	T-YSI
64	04/16/2013	62	0.54	4.01	4.55	11.0	88.0	28	36	int. grab

70	04/23/2013	86	9.57	13.51	23.08	41.0	58.0	28	36	int. grab
79	06/24/2013	9	0.01	0.13	0.14	7.0	92.0	32	77	T-OBS
80	07/02/2013	13	0.02	0.28	0.3	5.0	94.0	32	77	T-OBS
106	02/14/2014	25	0.26	1.57	1.82	14.0	85.0	32	51	T-OBS
107	02/15/2014	7	0.04	0.63	0.67	6.0	93.0	32	51	T-OBS
109	02/18/2014	12	0.01	0.81	0.81	0.0	99.0	32	51	T-OBS
110	02/20/2014	29	0.13	3.71	3.84	3.0	96.0	32	51	T-OBS
111	02/21/2014	51	2.55	7.03	9.58	26.0	73.0	32	51	T-OBS
112	02/24/2014	16	0.09	0.56	0.65	13.0	86.0	32	51	T-OBS
113	02/24/2014	1	0.01	0.12	0.13	9.0	90.0	32	51	T-OBS
114	02/25/2014	67	0.62	7.17	7.79	7.0	92.0	32	51	T-OBS
115	02/27/2014	16	0.13	0.68	0.8	15.0	84.0	32	51	T-OBS
116	02/27/2014	12	0.12	1.25	1.37	8.0	91.0	32	51	T-OBS
Total/Avg	42	1004	17.0	112.2	129.2	13	87	43	94	-
Tons/km2	-	-	18.8	127.5	72.6	-	-	-	-	-
DR	-	-	1	6.8	3.9	-	-	-	-	-

a. PE is cumulative probable error (Eq 6) as a percentage of the mean observed SSY.

b. Measured SSY_{EV} at FG1.

c. SSY_{EV} at FG3 - SSY_{EV} at FG1.

d. SSY_{EV} at FG3.

Table

Click here to download Table: Table3_S_budget_analysis_pre.pdf

Table 3. Total Suspended sediment yield (SSY), specific suspended sediment yield (sSSY), and disturbance ratio (DR) from disturbed portions of UPPER and LOWER subwatersheds for the storm events in Table 2.

	UPPER[a]	LOWER	TOTAL
Fraction of subwatershed area disturbed (%)	0.4	10.1	5.2
SSY (tons)	17.0	112.2	129.2
Forested areas	16.9	14.9	31.7
Disturbed areas	0.1	97.3	97.5
% from disturbed areas	0.9	87	75
sSSY, disturbed areas (tons/km^2)	41.0	1095.0	1053.1
DR for sSSY from disturbed areas[b]	2	58	56

a. Disturbed areas in UPPER are bare areas from landslides.

b. Calculated as (sSSY from disturbed areas)/sSSY from UPPER (17.0 tons/km^2)

Table

Click here to download Table: Table4_S_budget_2_pre.pdf

Table 4. Event-wise suspended sediment yield (SSYEV) from subwatersheds in Faga'alu for events with simultaneous data from FG1, FG2, and FG3. Storm numbers correspond with the storms presented in Table 2 and Appendix Table A3.1.

	Storm	Precip	SSY_{EV} tons					% of SSY_{EV} TOTAL			
Storm#	Start	mm	UPPER[a]	LOWER_QUARRY[b]	LOWER_VILLAGE[c]	LOWER[d]	TOTAL[e]	UPPER	LOWER_QUARRY	LOWER_VILLAGE	LOWER
2	01/19/2012	18	0.06	0.3	0.33	0.63	0.69	8.0	43.0	47.0	91.0
64	04/16/2013	62	0.54	2.77	1.24	4.01	4.55	11.0	60.0	27.0	88.0
70	04/23/2013	86	9.57	8.21	5.3	13.51	23.08	41.0	35.0	22.0	58.0
106	02/14/2014	25	0.26	1.01	0.55	1.57	1.82	14.0	55.0	30.0	86.0
110	02/20/2014	29	0.13	1.6	2.11	3.71	3.84	3.0	41.0	54.0	96.0
111	02/21/2014	51	2.55	2.07	4.96	7.03	9.58	26.0	21.0	51.0	73.0
115	02/27/2014	16	0.13	0.08	0.59	0.68	0.8	16.0	9.0	73.0	85.0
116	02/27/2014	12	0.12	0.32	0.93	1.25	1.37	8.0	23.0	67.0	91.0
Total/Avg	8	299	13.4	16.4	16.0	32.4	45.7	29	36	35	71
Tons/km2			14.8	60.6	26.7	36.8	25.7	-	-	-	-
DR			1.0	4.08	1.8	2.5	1.7	-	-	-	-

a. Measured SSY_{EV} at FG1.

b. SSY_{EV} at FG2 - SSY_{EV} at FG1.

c. SSY_{EV} at FG3 - SSY_{EV} at FG2.

d. SSY_{EV} at FG3 - SSY_{EV} at FG1.

e. Measured SSY_{EV} at FG3.

Table

Click here to download Table: Table5_S_budget_2_analysis_pre.pdf

Table 5. Total Suspended sediment yield (SSY), specific suspended sediment yield (sSSY), and disturbance ratio (DR) from disturbed portions of UPPER and LOWER subwatersheds for the storm events in Table 4.

	UPPER	LOWER_QUARRY	LOWER_VILLAGE	LOWER	TOTAL
Fraction of subwatershed area disturbed (%)	0.4	6.5	11.7	10.1	5.2
SSY (tons)	13.4	16.4	16.0	32.4	45.7
Forested areas	13.3	3.7	7.8	11.7	25.0
Disturbed areas	0.1	12.7	8.2	20.7	20.7
% from disturbed areas	1.0	77	51	64	45
sSSY, disturbed areas (tons/km^2)	37.0	721.6	116.2	232.8	223.9
DR for sSSY from disturbed areas	3	49	8	16	15

Table

Click here to download Table: Table6_All_Models_stats_pre.pdf

Table 6. Goodness-of-fit statistics for SSY_{EV} - storm metric relationships. Pearson and Spearman correlation coefficients signifcant at $p<0.01$.

Model	Pearson	Spearman	r^2	RMSE(tons)	Intercept(α)	Slope(β)
Psum_upper	-	0.70	0.39	4.31	0.003	1.10
Psum_total	0.84	0.88	0.71	2.43	0.033	1.11
EI_upper	0.42	0.48	0.18	5.48	0.001	0.97
EI_total	0.74	0.73	0.55	2.98	0.001	1.32
Qsum_upper	0.91	0.91	0.83	2.15	0.000	1.65
Qsum_total	0.84	0.83	0.70	2.46	0.000	1.29
Qmax_upper	0.89	0.90	0.79	2.36	0.398	1.51
Qmax_total	0.82	0.80	0.67	2.59	2.429	1.41

Table

Click here to download Table: Table7_Est_Annual_SSY_pre.pdf

Table 7. Estimates of Annual SSY and sSSY calculated using four different methods

	Psum model, Events in 2014	Qmax model, Events in 2014	Equation 5		
			Events in Table 2	Events in Table 4	All Measured Events
Precipitation					
mm (% of Ps_{ann})	2770	2770	1004 (36%)	299 (11%)	3457 (125%)
Annual SSY (tons/year)					
UPPER	13	61	50	120	41
LOWER	121	378	310	300	388
LOWER_QUARRY	-	-	-	150	-
LOWER_VILLAGE	-	-	-	150	-
TOTAL	134	439	360	420	428
Annual sSSY (tons/km^2/year)					
UPPER	14	68	50	140	45
LOWER	488	430	350	340	441
LOWER_QUARRY	-	-	-	560	-
LOWER_VILLAGE	-	-	-	250	-
TOTAL	75	247	200	240	241

Table

Click here to download Table: Table8_Lit_values_for_SSY.pdf

Table 8. Annual Specific Suspended Sediment Yield (sSSY) from steep, volcanic islands in the tropical Pacific.

Location	Watershed drainage area (km2)	Mean annual precipitation (mm)	sSSY range tons/km2/yr	Reference
Faga'alu UPPER	0.88		45-68	This study
Faga'alu TOTAL	1.78	2.380-6,350 (varies with elevation)	241-247	This study
Kawela, Molokai	13.5	500-3,000 (varies with elevation)	394	(Stock and Tribble, 2010)
Hanalei, Kauai	60.04	500 – 9,500 (varies with elevation)	545 ± 128	(Ferrier et al., 2013)
Hanalei, Kauai	48.4	2,000-11,000 (varies with elevation)	525	(Stock and Tribble, 2010)
Hanalei, Kauai	54.4	2,000-11,000 (varies with elevation)	140±55	(Calhoun and Fletcher, 1999)
St. John, USVI[a]	3.5	1,300-1,400	18	(Ramos-Scharrón and Macdonald, 2007)
St. John, USVI	2.3	1,300-1,400	24	(Nemeth and Nowlis, 2001)
St. John, USVI	6	1,300-1,400	36	(Nemeth and Nowlis, 2001)
Oahu	10.4	1,000-3,800 (varies with elevation)	330±130; 200±100 (varies with method)	(Hill et al., 1997)
Barro Colorado, Panama	0.033	2,623±458	100-200	(Zimmermann et al., 2012)
Fly River, PNG[b]	76,000	up to 10,000	1,000-1,500	(Milliman, 1995)
Purari River, PNG	35,000		3,000	"

Milliman and Syvitski (1992) Model: **sSSY = cA**[f] *c,f = regression coeff. for region/max elevation*		**c**	f	**sSSY tons/km2/yr**	(Milliman and Syvitski, 1992)
Max elev >3,000m	Faga'alu UPPER = 0.88 TOTAL = 1.78	280	-0.54	UPPER = 296 TOTAL = 205	-
Max elev 1000-3000m (Oceania)		65	-0.46	UPPER = 68 TOTAL = 50	-
Max elev 500-1,000m		12	-0.59	UPPER = 13 TOTAL = 9	-